ARTICLE

Ice-sheet collapse and sea-level rise at the Bølling warming 14,600 years ago

Pierre Deschamps[1], Nicolas Durand[1], Edouard Bard[1], Bruno Hamelin[1], Gilbert Camoin[1], Alexander L. Thomas[2], Gideon M. Henderson[2], Jun'ichi Okuno[3,4] & Yusuke Yokoyama[3,5]

Past sea-level records provide invaluable information about the response of ice sheets to climate forcing. Some such records suggest that the last deglaciation was punctuated by a dramatic period of sea-level rise, of about 20 metres, in less than 500 years. Controversy about the amplitude and timing of this meltwater pulse (MWP-1A) has, however, led to uncertainty about the source of the melt water and its temporal and causal relationships with the abrupt climate changes of the deglaciation. Here we show that MWP-1A started no earlier than 14,650 years ago and ended before 14,310 years ago, making it coeval with the Bølling warming. Our results, based on corals drilled offshore from Tahiti during Integrated Ocean Drilling Project Expedition 310, reveal that the increase in sea level at Tahiti was between 12 and 22 metres, with a most probable value between 14 and 18 metres, establishing a significant meltwater contribution from the Southern Hemisphere. This implies that the rate of eustatic sea-level rise exceeded 40 millimetres per year during MWP-1A.

Although dynamic responses of the Greenland and Antarctic ice sheets to climate forcing may already be contributing to present-day sea-level rise[1], projections of sea-level change for the twenty-first century do not fully include potential changes in ice dynamics[2]. As acknowledged by the IPCC[3], the vulnerability of Greenland and Antarctica to ongoing warming and related discharge feedbacks remains a major source of uncertainty in projected sea-level rise[4]. Reconstructions of past sea-level changes have provided evidence for large-amplitude and rapid discharges of fresh water from continental ice sheets. Several sea-level records suggest that the glacioeustatic rise following the Last Glacial Maximum (LGM) was characterized by brief periods of extremely rapid sea-level rise[5–10]. These short-term events, referred to as meltwater pulses, probably disturbed oceanic thermohaline circulation and global climate during the last deglaciation[11,12]. The exact chronology, origin and consequences of these ice-sheet melting episodes remain unclear. But understanding these episodes is of the utmost importance when considering current uncertainty surrounding potential collapse of large ice sheets in response to recent climate change[13].

The most extreme deglacial event, MWP-1A, was initially identified in the coral-based sea-level record from Barbados[5], where a sea-level rise of ~20 m was inferred between 14,100 and 13,600 years before present (14.1–13.6 kyr BP; from here on, all ages are given as kyr before present (BP), where 'present' refers to AD 1950)[6]. However, this event remains mysterious. Several records bear witness to its occurrence[8,14,15], although no broad agreement has emerged regarding its timing. Because of this lack of consensus, the temporal relationship between MWP-1A and abrupt (millennial-timescale) climatic events that punctuated the last deglaciation are the subject of considerable debate[12,16]. Additionally, the location(s) of melting ice responsible for this prominent feature of the last deglaciation remains elusive[17].

Two conflicting scenarios have been proposed to link the timing and source(s) of MWP-1A to the climatic history of the last deglaciation. On the basis of the Barbados record's chronology[5,6], it was initially argued that this episode of rapid sea-level rise was caused by a partial melting of Northern Hemisphere ice sheets (NHIS)[5,18,19]. This 'Northern' scenario was consistent with results from a coupled ocean–atmosphere general circulation model (GCM), in which massive freshwater input to the North Atlantic would result in a weakening of the Atlantic meridional overturning circulation (AMOC) and, through the reduction of deepwater formation in the Nordic Seas, the rapid cooling of the Northern Hemisphere[11]. In this scenario, MWP-1A may have initiated the Older Dryas cold event that abruptly ended the Bølling warming about 14.1 kyr ago[14,16].

In contrast, an alternative scenario points towards an Antarctic ice sheet (AIS) as the source of MWP-1A[17,20] and suggests a causative coupling between MWP-1A and the Bølling warm period[21]. This 'Southern' scenario suggests that MWP-1A coincided with an intensification of the thermohaline circulation at the onset of the Bølling warm period[22], rather than with a slowdown during the following cold event as predicted by the 'Northern' scenario. The 'Southern' scenario was supported by output from a GCM model of intermediate complexity showing that an MWP-1A originating from the West Antarctica Ice Sheet (WAIS) may have triggered sudden reactivation of the AMOC to lead to the Bølling warming[12]. Although still contentious, this scenario solves the apparent conundrum of the Bølling warming by providing a plausible triggering mechanism for the onset of this event, traditionally considered as marking the termination of the last glacial period.

The Tahiti record

Here we report U–Th dating of coral samples collected from the Tahiti reef slope during the Integrated Ocean Drilling Program (IODP) Expedition 310, 'Tahiti Sea Level'[23]. Tahiti is a far-field site located at a considerable distance from major former ice sheets and is characterized by slow and regular subsidence rates of ~0.25 mm yr^{-1}, as consistently assessed by several approaches. Considering a total range of 0.2–0.4 mm yr^{-1} suggested by these approaches, the uncertainty on the assessment of the MWP-1A amplitude, arising from the correction of island subsidence during MWP-1A, is entirely negligible (see Supplementary Information). Previous reconstructions of the

deglacial sea-level rise were established from holes drilled onshore through the modern barrier-reef in front of Papeete harbour[14,24]. The record was continuous from 13.9 kyr ago to present, but did not reach the critical MWP-1A period.

A specific target of Expedition 310 was the extension of the previous Tahiti sea-level record to cover earlier portions of the deglaciation. This was performed by offshore drilling of the Tahitian fore-reef slopes seaward of the present-day barrier reef (Fig. 1). These coring operations[23] recovered more than 400 m of post-glacial reef material, ranging from 122 to 40 metres below modern sea level (m.b.s.l.) in three distinct areas (Maraa, Faaa and Tiarei) around Tahiti (Fig. 1).

Our reconstruction of sea level relies on absolute U–Th dating of corals, belonging to coralgal (that is, coral and algal) assemblages indicative of a range of modern reef environments, from the shallow reef crest to the deepest reef slope. Eighty U–Th ages were determined on coral samples recovered from twenty-three holes drilled at fourteen different sites. These new data extend the Tahiti record to cover the last 16 kyr BP (Fig. 2), and provide a complete and detailed record of sea-level rise during this key period of the last deglaciation. In each hole, all of the ages are in stratigraphic order (Supplementary Fig. 2). However, even for the closely spaced holes, significant differences in recorded water depths may be observed (see, for example, the difference recorded between Site M0024 versus Site M0009 that may be up to ~10 m; Supplementary Fig. 2). The depth distribution observed for the various coral species analysed here is broadly consistent with their present-day biological zonation (Supplementary Fig. 4). The large number of holes drilled in the fore-reef slope, as well as their widespread distribution, ensured the recovery of the depth distribution of reef diversity and varying responses of reef development to sea-level rise. Our observations compare favourably with a reef accretion model[25], suggesting heterogeneous reef development induced by multiple factors including the following: spatially random (patchy) colonization; varying accretion patterns; and rugged topography of the pre-glacial surface that partially controlled the post-glacial reef initiation and growth following flooding. Our record, based on several contemporaneous cores, is therefore more representative than a record derived from a single drill hole which may provide a misleading impression of reef response to sea-level rise[25].

Sea–level rise during early deglaciation

The two oldest samples, dated at 15.74 ± 0.03 kyr BP and 16.09 ± 0.04 kyr BP, are robust branching *Pocillopora* collected at the interface of the underlying Pleistocene unit in cores 24A-15R and 9B-15R. These samples belong to a shallow-water coralgal assemblage, <10 metres water depth (m.w.d.), and indicate a Relative Sea Level (RSL) of 117–107 m.b.s.l. during that time. This RSL estimate is strengthened by the presence of an encrusting *Montipora* collected at a subsidence-corrected depth of 114 m.b.s.l. in core 25B-11R. Dated at 15.31 ± 0.02 kyr BP, this sample is associated with vermetid gastropods that are indicative of a very shallow environment (<~5 m.w.d.)[26]. From these observations, we may infer an RSL of 117–109 m.b.s.l. during the early part of the deglaciation at Tahiti (see Fig. 2).

Because of glacial isostatic adjustment (GIA), the RSL records from different sites cannot be compared directly, even in far-field regions[20]. For the time window 14–20 kyr BP, GIA models produce an RSL that is lower at Tahiti than eustatic sea level[20,27], in contrast to other sites commonly used for the analysis of sea-level change (Barbados, Bonaparte Gulf and Huon Peninsula) where GIA effects lead to local sea level lying above the eustatic value. By taking this factor into account, our 117–109 m.b.s.l. RSL estimate at 16 kyr BP is therefore in good agreement with observations from the Sunda Shelf (Supplementary Fig. 8) for the same period[8]. RSL observations from Barbados and Bonaparte Gulf display a dense cluster of samples dated at about 18–19 kyr BP, which strongly constrains eustatic sea level to a depth less than 110 m in this interval[28]. Therefore, a comparison with our data suggests that, during the early stage of deglaciation, after the MWP that occurred at 19 kyr BP[9,10], the eustatic sea level (ESL) remained stable or rose only slightly during the time span surrounding the Heinrich 1 event (probably no more than 5 m for ~3 kyr).

For the time window spanning 16.1–14.6 kyr BP, hole 24A (from the outer ridge at Tiarei) delineates the lower envelope of sea-level change. In this hole, coralgal assemblages are indicative of a very shallow environment and were able to keep pace with rising sea level during this period. The pre-MWP-1A RSL is well constrained by three coral samples collected at a subsidence-corrected depth of 105 m.b.s.l.: a massive *Montipora* sample dated at 14.65 ± 0.02 kyr BP in core 15A-37R from Maraa; and two robust branching *Pocillopora* samples dated at 14.58 ± 0.05 kyr BP and 14.61 ± 0.03 kyr BP in core 24A-10R from Tiarei (see Supplementary Information and Supplementary Fig. 3). These two last corals belong to a coralgal assemblage that typifies a shallow-water environment of less than 10 m.w.d. and are associated with vermetids that are indicative of shallow-water conditions (<~5 m.w.d.)[26]. This places a conservative constraint of 105–100 m.b.s.l. on the pre-MWP-1A sea level at 14.65 kyr BP. A moderate
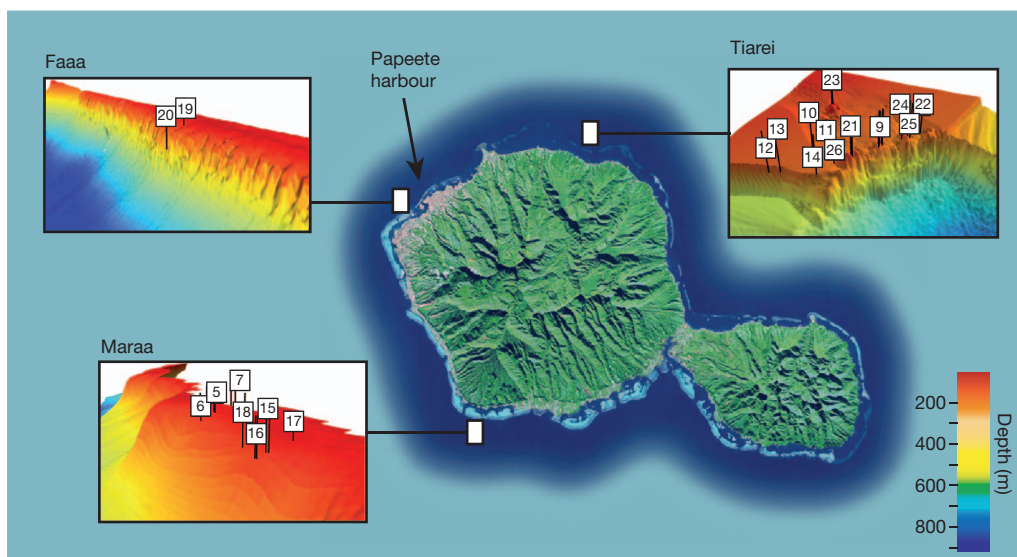

Figure 1 | A Landsat image of Tahiti island. Shown are the locations of the three areas (Tiarei, Maraa and Faaa) drilled during IODP Expedition 310, as well as Papeete harbour where onshore holes were drilled previously. A total of 37 boreholes were cored during IODP 310 at 22 different sites providing more than 400 m of post-glacial reef material[23]. Insets show the bathymetry for each site, with the location of the different drilled holes.
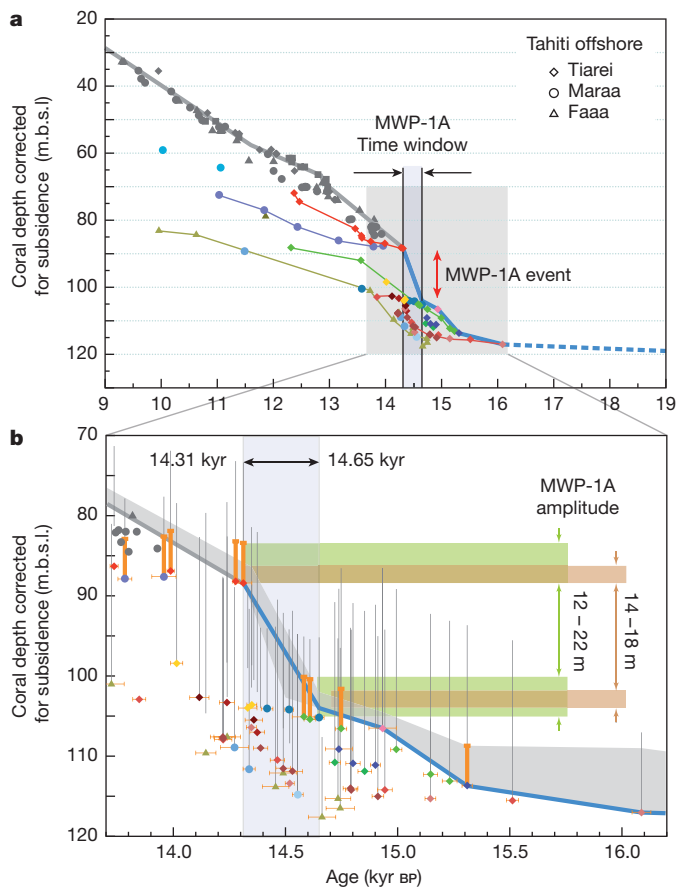
Figure 2 | The deglacial Tahiti sea-level curve. a, Sea level reconstructed from U–Th dated corals recovered in long holes drilled onshore and offshore Tahiti island. Coral depths are expressed in metres below present sea level (m.b.s.l.) and are corrected for a constant subsidence rate of 0.25 mm yr^{-1} (see Supplementary Information). Grey and coloured symbols show respectively coral samples collected in onshore holes[14,24] and in offshore holes drilled during IODP Expedition 310. Red diamonds show key samples from the inner ridge of Tiarei (Site M0023). Thick blue line shows the lower estimate of the Tahiti RSL curve (see Supplementary Information); it extends the grey curve determined by linear fits of onshore sea-level data[24] and clearly indicates the occurrence of a rapid rise of the sea level (orange arrow) related to the MWP-1A event. The shaded time window and black arrows highlight the tight chronological constraints derived for MWP-1A from the Tahiti record. **b,** Magnified view of the MWP-1A time window. The vertical grey bars reported for each coral sample correspond to their optimal bathymetric habitat range inferred from the coralgal assemblage identification (see Supplementary Information) and thick orange bars indicate samples associated with vermetid gastropods that are indicative of a shallow environment (0–5 m.w.d.). The shaded grey band illustrates our estimate of the most likely range of the Tahiti RSL over the last deglaciation. The ranges of uncertainty estimated from the bathymetric range of coralgal assemblages for the pre- and post-MWP-1A sea-level positions are illustrated by the horizontal green bands. The resulting extreme bounds for the MWP-1A amplitude (12 and 22 m) are also indicated (green bands and arrows). Several arguments given in the Supplementary Information suggest that these conservative estimates can be trimmed to 14 and 18 m (brown bands and arrows). Thick blue line and thick grey line are as in **a**.

sea-level rise of 4–14 m is therefore inferred for the period from 16.1 to 14.65 kyr BP.

The earliest bound for the initiation of the MWP-1A jump of sea level is probably within the time range given by those three samples (14.58–14.65 kyr BP). Moreover, the two *Pocillopora* samples dated at 14.58 and 14.61 kyr BP could have already grown at a reasonable water depth (up to 5 m.w.d.). Thus, they may have already accommodated a part of the sea-level rise related to MWP-1A, implying that the inception of MWP-1A could have occurred somewhat earlier (see the upper

bound of the shaded grey area in Fig. 2; see also Supplementary Fig. 4). The maximum age for the onset of MWP-1A could thus be close to the oldest of these three corals, dated at 14.65 kyr BP. It must be emphasized that this only provides us with the uppermost limit for the onset of MWP-1A, and we cannot rule out that the jump may have started significantly later, as young as 14.5 kyr BP, as potentially marked by massive *Montipora* samples of core 15A-36R that characterize a shallow environment (see Supplementary Figs 3–5).

Occurrence of MWP-1A

The occurrence of MWP-1A is revealed by a major discontinuity in the upper envelope of the data points in the new Tahiti RSL record (Fig. 2). The next shallowest *in situ* samples in the sequence are two branching *Pocillopora* dated at 14.28 ± 0.02 kyr BP and 14.31 ± 0.04 kyr BP in cores 23B-12R and 23A-13R (see Supplementary Information and Supplementary Fig. 3). These coral samples, recovered at a subsidence-corrected depth of 88 m.b.s.l., are the first datable corals, showing clear evidence of an in-growth position, to colonize the pre-glacial substratum after the MWP-1A sea-level jump. These samples are critical, as they provide the most robust constraint on MWP-1A timing and clearly indicate that the sea-level jump was complete before 14.31 kyr BP. These data lie on the extension of the general trend depicted by onshore holes[14,24] (Fig. 2) and highlight a regular, slow rate of sea-level rise after MWP-1A. These corals are associated with vermetids, thus indicating a very shallow environment (<~5 m.w.d.). We infer a conservative estimate of 88–83 m.b.s.l. for the post-MWP-1A sea level.

The MWP-1A event also coincides with a major change in reef development strategy, as illustrated by numerous samples dated in all drill holes collected on the outer edge of the fore-reef slopes. Before MWP-1A the reef kept pace with sea level, whereas a widespread deepening and backstepping occurred after MWP-1A. This change in reef response is coincident with changes in the coralgal assemblage composition, such as in Hole M0024A (see Supplementary Information and Supplementary Fig. 3), where shallow-water assemblages—dominated by robust branching *Pocillopora*, massive *Porites* and encrusting *Montipora*—change to branching *Porites* species, which typify an environment characterized by moderate energy and light intensity.

General features of reef geometry can be simulated with a two-dimensional growth model[14]. This model simulates the overall deepening of the reef sequence that follows occurrence of a rapid sea-level rise and clearly indicates that only holes drilled in the intermediate position between the outer ridge and the modern barrier reef are capable of capturing the sea-level position immediately following MWP-1A (see Supplementary Figs 9 and 10). This result probably explains the difficulty encountered by previous onshore or offshore drilling programmes (Tahiti or Barbados) to collect shallow-species coral samples that document precisely the end of MWP-1A. The IODP Mission Specific Platform overcame this difficulty by specifically targeting the reef structures located in intermediate position between the fore-reef slope and the present barrier reef, especially at the Tiarei site.

Amplitude and duration of MWP-1A at Tahiti

On the basis of the most conservative estimates deduced above for the pre- and post-MWP-1A sea level, we infer an amplitude of 17 m for the sea-level jump, with lowest and uppermost bounds of 12 and 22 m. Several arguments, discussed in detail in Supplementary Information (Supplementary Fig. 6), suggest that this range may reasonably be narrowed down to 14–18 m, with a median value of 16 m.

In view of the lower and upper limits of the MWP-1A chronozone (14.31 kyr BP and 14.65 kyr BP, respectively), the longest possible duration of the jump is ~350 years (Fig. 3). Considering the median value of 16 m for the local amplitude of MWP-1A at Tahiti, we infer an average RSL rate of ~46 ± 6 mm yr^{-1} at Tahiti. However, owing to the age uncertainty associated with its inception and termination (see
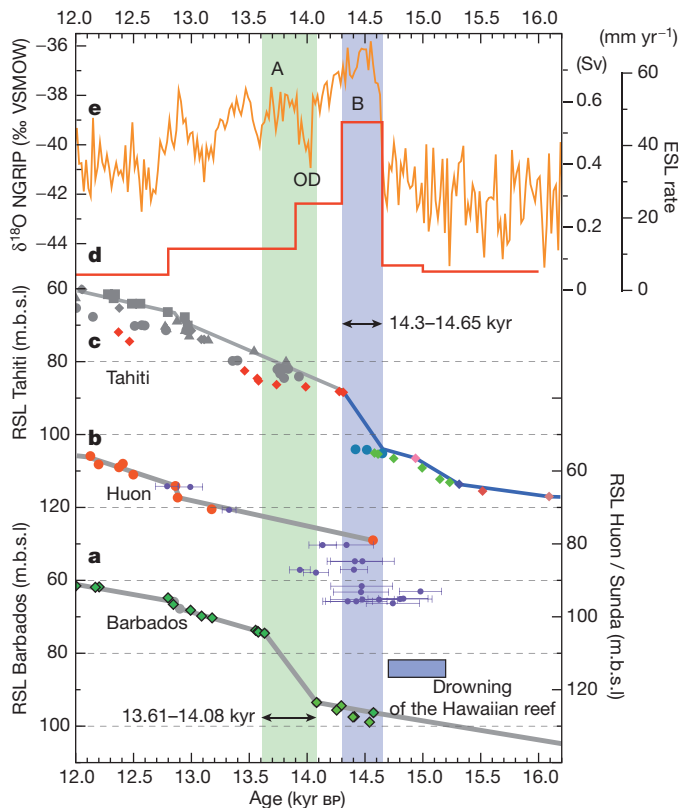
Figure 3 | Relative sea-level (RSL) records over the time window 16.5 to 12.0 kyr BP. a, Barbados RSL record based on U–Th dated corals (mainly *Acropora palmata*)[19,29]. The shaded green vertical band highlights the MWP-1A time window inferred from the Barbados record[19,29] **b,** Pacific RSL records (right-hand vertical axis). Red circles, Huon Peninsula record[31,32] (Papua New Guinea) based on U–Th dated corals. Purple points, Sunda Shelf record[8] based on ^{14}C-dated organic material found in sediment cores (recalibrated using IntCal09[30]; plotted errors are 1σ). The blue rectangle indicates the drowning of a Hawaiian reef 14.7 kyr ago[15]. **c,** Tahiti RSL record based on U–Th dated corals collected in holes drilled onshore (grey symbols)[14,24] and offshore (coloured symbols, this study). The shaded purple vertical band highlights the MWP-1A time window inferred from this study. **d,** Rate of glacial meltwater discharge (expressed in mm yr^{-1} and Sv, right-hand vertical axes) derived from the eustatic sea level curve determined by the GIA model (see Supplementary Information and Supplementary Fig. 11) adjusted to account for the newly obtained timing and magnitude of MWP-1A from Tahitian sea-level observations. **e,** δ^{18}O record of the North Greenland Ice Core Project (NGRIP) core plotted on its most recent timescale[34]; B, Bølling; OD, Older Dryas; A, Allerød. All depths have been corrected for subsidence (Tahiti) and uplift (all other sites) as described in ref. 24. For Tahiti and Barbados records, only samples that delineate the upper envelope are shown. Grey lines correspond to linear fits of sea-level data[24]. Greenish and bluish shaded time windows correspond to MWP-1A chronozones inferred from the Barbados record and the Tahiti record (Fig. 2), respectively.

Supplementary Information), the MWP-1A duration could have been even shorter than this estimate. An extremely sharp meltwater outburst, of the order of a century or less, is thus possible, in which case the 46 mm yr^{-1} rate of sea-level rise must be considered as a minimum value.

Timing of MWP-1A

The new MWP-1A chronozone inferred from the extended Tahiti record (that is, 14.65–14.31 kyr BP or shorter, Fig. 3) does not overlap with that previously proposed on the basis of the Barbados record (14.08 ± 0.06 to 13.63 ± 0.03 kyr BP, using the most recent updated data set[19,29]; see Supplementary Information for a full discussion of this issue).

Several other lines of evidence also suggest that MWP-1A was significantly older than suggested by the Barbados record and, ultimately, concurrent with the Bølling warming. Additional evidence comes from the Sunda Shelf sea-level record, derived from mangrove organic material collected from a shallow siliciclastic platform[8]. This record shows a very sharp sea-level rise dated at a conventional ^{14}C age of 12.42 ± 0.06 kyr BP (1 s.d., $n = 17$; Supplementary Fig. 8) coinciding with the 500-year-long ^{14}C plateau that encompasses the Bølling period. Using the IntCal09 calibration curve[30], the mean calendar age of the MWP-1A event recorded on the Sunda Shelf can be refined to 14.94–14.14 kyr cal. BP (2σ interval, see Supplementary Information for more details regarding this age calculation).

The revised MWP-1A timescale inferred from the new Tahiti record is also coherent with the recent extension of the Huon Peninsula record[31,32], where the oldest sample of the post-glacial reef sequence dated at 14.56 ± 0.05 kyr BP places an upper constraint on the end of MWP-1A (Fig. 3). Further indirect evidence is provided by the drowning of coral reefs offshore from Hawaii, which occurred at 14.7 kyr BP and has been proposed to be caused by a dramatic increase in sea level related to MWP-1A[15].

These records are consistent enough to revise the onset of MWP-1A so it is 500 years earlier than the date inferred from the Barbados data. Within this revised timeframe, MWP-1A can no longer be advocated as the trigger for the Older Dryas cooling event that terminated the Bølling period, as proposed previously[14,16,33]. Instead, MWP-1A coincided with the inception of the Bølling period (Fig. 3), which has been independently constrained by the GICC 05 Greenland ice core chronology at 14.640 kyr BP (with a maximum counting error of 0.186 kyr)[34]. The Tahiti record is thus compatible with the idea of a temporal relationship between MWP-1A and Bølling warming. This hypothesis is further substantiated by the concurrent occurrence of rapid flooding on shelf margins and an increase in sea surface temperature in the South China Sea at the Bølling transition[21].

Source of MWP-1A

Because they account for more than 80% of total sea-level rise during the last deglaciation, NHIS, and especially the Laurentide Ice Sheet (LIS), have commonly been considered as the sole sources for MWP-1A[5,35]. But arguments for such an LIS source faced serious objections, and led to the proposal[17] of an alternative scenario in which a significant fraction of the melt water came from Antarctica.

Direct evidence in favour of a Northern or Southern Hemisphere source remains equivocal. Most robust arguments supporting an Antarctic contribution were provided by GIA models[20,36,37]. Fingerprinting model experiments demonstrated that comparison of the size of the MWP-1A sea-level rise observed at several sites could provide helpful information about the source(s) of melting ice[36]. Predictions provided in ref. 36 showed that, when melting ice originated exclusively from the LIS, the amplitude of MWP-1A predicted for Barbados should be significantly lower than for far-field sites. This scenario predicted the greatest difference in amplitude between Barbados and Tahiti, with a sea-level rise at Tahiti almost twice that at Barbados[36].

The amplitude of MWP-1A that we assess at Tahiti (16 m) is comparable to that observed at Sunda (~16 m)[8]. At Barbados, the amplitude of the jump must be reassessed on the basis of the re-evaluation of the MWP-1A chronozone (Supplementary Fig. 7). By extrapolating the linear trend defined by hole 12 (Supplementary Fig. 7), we roughly estimate a ~15 m amplitude of sea-level rise at Barbados. The amplitudes of MWP-1A recorded at these three far-to-intermediate-field sites are thus approximately the same. Following the predictions of ref. 36, our results seem to preclude a sole LIS contribution to MWP-1A and confirm the preliminary conclusions[36] based solely on the Sunda and Barbados records. On this basis, the Barents and Fennoscandian Ice Sheets can also be considered as possible candidates for the freshwater source (see figure 2 in ref. 36), but there are

several counterarguments to these ice sheets as the major sources of fresh water[17]. All other scenarios that provide equal amplitudes of MWP-1A sea-level rise require a significant Antarctic contribution.

These arguments in favour of a contribution from the AIS were reinforced by GIA predictions[20]. Those predictions showed that the optimal deglacial scenario to fit RSL observations at Barbados, Tahiti, Huon Peninsula and Sunda Shelf during late glacial time required a MWP-1A with a total amplitude of 23 m, which included an AIS contribution of 15 m with a total NHIS contribution of 8 m (6 m from the LIS).

Using a realistic GIA model (see Supplementary Fig. 11 and Supplementary Information), which uses the Earth model proposed in ref. 20, we performed a new set of simulations that agree well with the conclusion of Bassett *et al.*[20], pointing towards a substantial contribution from the AIS. It is difficult at this stage, however, to conclusively determine the relative contributions of NHIS and the AIS to MWP-1A because these approaches (fingerprinting and more general GIA modelling) are hampered by uncertainties surrounding the MWP-1A-induced relative sea-level amplitude, especially at the intermediate-field site of Barbados. Following previous studies[27,36], which conclude that the MWP-1A amplitude recorded at Tahiti is amplified by 10–30% with respect to its eustatic amplitude, our results are consistent with a eustatic MWP-1A rise of roughly ~14 m during the time window 14.65–14.3 kyr BP, leading to a rate of eustatic sea level rise of 40 mm yr^{-1}. Note that this value is significantly lower than the 20–25 m of eustatic rise often reported in the literature[20,36]. Considering the growing body of evidence[20,36,37] that suggests that a substantial fraction of MWP-1A originated from Antarctica, it is probable that the AIS contributed at least half of the ~14 m eustatic sea-level rise observed during this event. It is worth noting that this estimate of the Antarctic contribution allows us to balance the freshwater budget required for MWP-1A, taking into account NHIS contributions that have been independently assessed to be between 5 and 10 m of sea-level equivalent ice volume[38,39]. Recent estimates of AIS contribution to the last deglaciation indicate that its contribution was <20 m and perhaps lower than 10–15 m (refs 40–42), implying that a significant, if not the major, part of the AIS contribution to the last deglaciation occurred during MWP-1A.

Implications of the revisited MWP-1A history

The IODP Expedition 310 provides significantly improved constraints on the timing of MWP-1A, demonstrating that MWP-1A ended before 14.3 kyr BP and that it started after 14.65 kyr BP. This makes MWP-1A coeval with the Bølling warming, suggesting a temporal, and probably causal, relationship between these two prominent deglacial features. Owing to the dating uncertainty of the Bølling inception in the Greenland ice record (14.642 kyr BP with a maximum counting error of 186 years; ref. 34), it remains difficult to unravel the phasing and causal mechanisms linking—through specific atmospheric and oceanic responses—the resumption of the AMOC during the Bølling warming[22] and massive meltwater discharges in both hemispheres. Two end-member scenarios that warrant further investigation can be put forward, however:

The first scenario is that proposed in ref. 12, based on GCM simulations showing that a rapid freshwater discharge originating from the AIS could have led to an intensification of the AMOC. The associated northward ocean heat flux would trigger the Bølling warming in the Northern Hemisphere and a rapid melting of the LIS. But subsequent studies (for example, ref. 43 and references therein) that have tested the scenario of ref. 12 showed that the meltwater discharge may have led to competing mechanisms, enhancing or weakening the AMOC, which collectively lead to a subdued climatic response in the Northern Hemisphere[43].

In the second scenario, the phasing of events is reversed, with an initial AMOC increase and associated northward ocean heat transport causing the Bølling warming, which led to rapid melting of NHIS,

in particular the LIS. The resulting sea-level rise drove in turn a dramatic collapse of the AIS. Indeed, the WAIS was partly marine-based during the LGM and thus probably sensitive to the break-up and loss of buttressing ice shelves. In any case, most of the WAIS is characterized by unstable conditions, with bedrock below sea level and slopes downward from the margins towards the interior[13].

In fact, these two scenarios are not mutually exclusive and could have acted in concert during the MWP-1A chronozone, reinforcing each other. They are both compatible with our sea-level and source fingerprinting study, which implies that meltwater injections forming the MWP-1A event originated from ice sheets in both Antarctica and the Northern Hemisphere, including the LIS. In principle, meltwater injection into the North Atlantic could have counteracted the AMOC increase, but the strength of this negative feedback depends on the exact location and mode of meltwater release. Several studies suggested that LIS meltwater was funnelled through the Mississippi drainage system, before being released in the Gulf of Mexico as a hyperpycnal flow[38,44], with a negligible impact on the AMOC[39,45,46].

The two scenarios have similar ingredients but differ in their ultimate trigger, AIS collapse or AMOC increase. These abrupt events could be linked to threshold responses to the gradual warming of the Southern Hemisphere that occurred under external forcings (orbital and greenhouse-gas changes) during the early part of the deglaciation[47,48].

Much research remains to be done to document the precise sequence of events during the MWP-1A chronozone. This will come from coring coral reefs at other sites (for example, Barbados and the Seychelles[27]), from study of open-ocean sediments in the vicinity of former ice sheets, and from modelling work to simulate the complex interplay between ice sheets, ocean and atmosphere. Whatever the causes that led to the MWP-1A event and the Bølling warming, and despite the fact that the total eustatic magnitude of this event is reduced compared to previous estimates, our results prove the existence of a dramatic collapse of past ice sheets at a eustatic rate exceeding 40 mm yr^{-1}, with a substantial contribution from Antarctica. We note that this rate is at least four time as large as the average rate of deglacial sea-level rise of ~10 mm yr^{-1}; see ref. 24 and Supplementary Information. Understanding this singular event will shed light on the dynamical behaviour of large ice sheets in response to external forcing or internal perturbation of the climate system. This topic is crucial in the context of the present warming, as modern ice sheets have been shown to be contributing directly to the recent acceleration in sea-level rise[1,2].

METHODS SUMMARY

Before U–Th dating, rigorous mineralogical and isotopic screening criteria were applied to discard coral samples that suffered any post-mortem diagenetic alteration of their aragonite skeleton. In particular, using X-ray diffraction[30], we made an effort to improve the detection and quantification of a very small amount of secondary calcite. Coral samples showing a calcite content of more than 1% were discarded. Most of the U–Th analyses were performed using a VG-54 thermo-ionization mass spectrometer equipped with a 30-cm electrostatic analyser and a pulse-counting Daly detector at CEREGE (see Supplementary Information for data and analytical issues). The initial $(^{234}U/^{238}U)_0$ values calculated for post-glacial samples yielded a mean value of 1.1458 ± 0.0020 (2σ), falling within the most recent determinations of modern sea water and corals[49]. Additionally, for corals of the same age, $(^{234}U/^{238}U)_0$ values were highly consistent (that is, within an analytical uncertainty determined for the entire course of the study of 0.8‰, 2σ), and within the larger range adopted[30] as an isotopic screening criterion in the interval 0–17 kyr BP ($(^{234}U/^{238}U)_0 = 1.1452 \pm 0.0048$, 2σ). The clustering of $(^{234}U/^{238}U)_0$ values determined in this study substantially narrows the uncertainty for the evolution of the seawater value through time compared to previous data sets (Vanuatu, Papua New Guinea and Barbados) that have encompassed the last deglaciation, highlighting the outstanding quality of the coral samples recovered in Tahiti offshore holes. Complementary and duplicated analyses were also performed by Multi-Collector Inductively Coupled Mass Spectrometry[50] and show a general good agreement within measurement uncertainties.

1. Milne, G. A., Gehrels, W. R., Hughes, C. W. & Tamisiea, M. E. Identifying the causes of sea-level change. *Nature Geosci.* **2**, 471–478 (2009).
2. Pfeffer, W. T., Harper, J. T. & O'Neel, S. Kinematic constraints on glacier contributions to 21st-century sea-level rise. *Science* **321**, 1340–1343 (2008).
3. Meehl, G. A. *et al.* in *Climate Change 2007: The Physical Science Basis* (eds Solomon, S. *et al.*) 747–845 (Cambridge Univ. Press, 2007).
4. Alley, R. B., Clark, P. U., Huybrechts, P. & Joughin, I. Ice-sheet and sea-level changes. *Science* **310**, 456–460 (2005).
5. Fairbanks, R. G. A 17,000-year glacio-eustatic sea level record; influence of glacial melting rates on the Younger Dryas event and deep-ocean circulation. *Nature* **342**, 637–642 (1989).
6. Bard, E., Hamelin, B. & Fairbanks, R. G. U-Th ages obtained by mass spectrometry in corals from Barbados: sea level during the past 130,000 years. *Nature* **346**, 456–458 (1990).
7. Blanchon, P. & Shaw, J. Reef drowning during the last deglaciation: evidence for catastrophic sea-level rise and ice-sheet collapse. *Geology* **23**, 4–8 (1995).
8. Hanebuth, T., Stattegger, K. & Grootes, P. M. Rapid flooding of the Sunda Shelf: a late-glacial sea-level record. *Science* **288**, 1033–1035 (2000).
9. Yokoyama, Y., Lambeck, K., De Deckker, P., Johnston, P. & Fifield, L. K. Timing of the Last Glacial Maximum from observed sea-level minima. *Nature* **406**, 713–716 (2000).
10. Clark, P. U., McCabe, A. M., Mix, A. C. & Weaver, A. J. Rapid rise of sea level 19,000 years ago and its global implications. *Science* **304**, 1141–1144 (2004).
11. Manabe, S. & Stouffer, R. J. Simulation of abrupt climate change induced by freshwater input to the North Atlantic Ocean. *Nature* **378**, 165–167 (1995).
12. Weaver, A. J., Saenko, O. A., Clark, P. U. & Mitrovica, J. X. Meltwater pulse 1A from Antarctica as a trigger of the Bølling-Allerød warm interval. *Science* **299**, 1709–1713 (2003).
13. Bamber, J. L., Riva, R. E. M., Vermeersen, B. L. A. & LeBrocq, A. M. Reassessment of the potential sea-level rise from a collapse of the West Antarctic Ice Sheet. *Science* **324**, 901–903 (2009).
14. Bard, E. *et al.* Deglacial sea-level record from Tahiti corals and the timing of global meltwater discharge. *Nature* **382**, 241–244 (1996).
15. Webster, J. M. *et al.* Drowning of the −150 m reef off Hawaii: a casualty of global meltwater pulse 1A? *Geology* **32**, 249–252 (2004).
16. Stanford, J. D. *et al.* Timing of meltwater pulse 1a and climate responses to meltwater injections. *Paleoceanography* **21**, PA4103, http://dx.doi.org/10.1029/2006PA001340 (2006).
17. Clark, P. U. *et al.* Origin of the first global meltwater pulse following the last glacial maximum. *Paleoceanography* **11**, 563–577 (1996).
18. Peltier, W. R. On the hemispheric origins of meltwater pulse 1a. *Quat. Sci. Rev.* **24**, 1655–1671 (2005).
19. Peltier, W. R. & Fairbanks, R. G. Global glacial ice volume and Last Glacial Maximum duration from an extended Barbados sea level record. *Quat. Sci. Rev.* **25**, 3322–3337 (2006).
20. Bassett, S. E., Milne, G. A., Mitrovica, J. X. & Clark, P. U. Ice sheet and solid earth influences on far-field sea-level histories. *Science* **309**, 925–928 (2005).
21. Kienast, M., Hanebuth, T. J. J., Pelejero, C. & Steinke, S. Synchroneity of meltwater pulse 1a and the Bølling warming: new evidence from the South China Sea. *Geology* **31**, 67–70 (2003).
22. McManus, J. F., Francois, R., Gherardi, J. M., Keigwin, L. D. & Brown-Leger, S. Collapse and rapid resumption of Atlantic meridional circulation linked to deglacial climate changes. *Nature* **428**, 834–837 (2004).
23. Camoin, G., Iryu, Y., McInroy, D., &. Expedition 310 Scientists. Expedition 310. *Proc. IODP* Vol. 310 *Expedition Reports* http://dx.doi.org/10.2204/iodp.proc.310.2007 (2007).
24. Bard, E., Hamelin, B. & Delanghe-Sabatier, D. Deglacial meltwater pulse 1B and Younger Dryas sea levels revisited with boreholes at Tahiti. *Science* **327**, 1235–1237 (2010).
25. Blanchon, P. & Blakeway, D. Are catch-up reefs an artefact of coring? *Sedimentology* **50**, 1271–1282 (2003).
26. Cabioch, G., Montaggioni, L. F., Faure, G. & Ribaud-Laurenti, A. Reef coralgal assemblages as recorders of paleobathymetry and sea level changes in the Indo-Pacific province. *Quat. Sci. Rev.* **18**, 1681–1695 (1999).
27. Milne, G. A. & Mitrovica, J. X. Searching for eustasy in deglacial sea-level histories. *Quat. Sci. Rev.* **27**, 2292–2302 (2008).
28. Peltier, W. R. On eustatic sea level history: Last Glacial Maximum to Holocene. *Quat. Sci. Rev.* **21**, 377–396 (2002).
29. Fairbanks, R. G. *et al.* Radiocarbon calibration curve spanning 0 to 50,000 years BP based on paired ^{230}Th/^{234}U/^{238}U and ^{14}C dates on pristine corals. *Quat. Sci. Rev.* **24**, 1781–1796 (2005).
30. Reimer, P. J. *et al.* Intcal09 and Marine09 radiocarbon age calibration curves, 0–50,000 years cal BP. *Radiocarbon* **51**, 1111–1150 (2009).
31. Edwards, R. L. *et al.* A large drop in atmospheric ^{14}C/^{12}C and reduced melting in the Younger Dryas, documented with ^{230}Th ages of corals. *Science* **260**, 962–968 (1993).
32. Cutler, K. B. *et al.* Rapid sea-level fall and deep-ocean temperature change since the last interglacial period. *Earth Planet. Sci. Lett.* **206**, 253–271 (2003).
33. Liu, J. P. & Milliman, J. D. Reconsidering meltwater pulses 1A and 1B: global impacts of rapid sea level rise. *J. Ocean Univ. China* **3**, 183–190 (2004).
34. Rasmussen, T. L. *et al.* A new Greenland ice core chronology for the last glacial termination. *J. Geophys. Res.* **111**, D06102, http://dx.doi.org/10.1029/2005JD006079 (2006).
35. Peltier, W. R. Ice-age paleotopography. *Science* **265**, 195–201 (1994).
36. Clark, P. U., Mitrovica, J. X., Milne, G. A. & Tamisiea, M. E. Sea-level fingerprinting as a direct test for the source of global meltwater pulse IA. *Science* **295**, 2438–2441 (2002).
37. Bassett, S. E., Milne, G. A., Bentley, M. J. & Huybrechts, P. Modelling Antarctic sea-level data to explore the possibility of a dominant Antarctic contribution to meltwater pulse IA. *Quat. Sci. Rev.* **26**, 2113–2127 (2007).
38. Carlson, A. E. Geochemical constraints on the Laurentide Ice Sheet contribution to Meltwater Pulse 1A. *Quat. Sci. Rev.* **28**, 1625–1630 (2009).
39. Tarasov, L. & Peltier, W. R. A calibrated deglacial drainage chronology for the North American continent: evidence of an Arctic trigger for the Younger Dryas. *Quat. Sci. Rev.* **25**, 659–688 (2006).
40. Clark, P. U. & Mix, A. C. Ice sheets and sea level of the Last Glacial Maximum. *Quat. Sci. Rev.* **21**, 1–7 (2002).
41. Denton, G. H. & Hughes, T. J. Reconstructing the Antarctic Ice Sheet at the Last Glacial Maximum. *Quat. Sci. Rev.* **21**, 193–202 (2002).
42. Bentley, M. J. The Antarctic palaeo record and its role in improving predictions of future Antarctic Ice Sheet change. *J. Quat. Sci.* **25**, 5–18 (2010).
43. Swingedouw, D., Fichefet, T., Goosse, H. & Loutre, M. F. Impact of transient freshwater releases in the Southern Ocean on the AMOC and climate. *Clim. Dyn.* **33**, 365–381 (2009).
44. Aharon, P. Entrainment of meltwaters in hyperpycnal flows during deglaciation superfloods in the Gulf of Mexico. *Earth Planet. Sci. Lett.* **241**, 260–270 (2006).
45. Roche, D. M., Renssen, H., Weber, S. L. & Goosse, H. Could meltwater pulses have been sneaked unnoticed into the deep ocean during the last glacial? *Geophys. Res. Lett.* **34**, L24708, http://dx.doi.org/10.1029/2007GL032064 (2007).
46. Tarasov, L. & Peltier, W. R. Arctic freshwater forcing of the Younger Dryas cold reversal. *Nature* **435**, 662–665 (2005).
47. Knorr, G. & Lohmann, G. Southern Ocean origin for the resumption of Atlantic thermohaline circulation during deglaciation. *Nature* **424**, 532–536 (2003).
48. Knorr, G. & Lohmann, G. Rapid transitions in the Atlantic thermohaline circulation triggered by global warming and meltwater during the last deglaciation. *Geochem. Geophys. Geosyst.* **8**, Q12006, http://dx.doi.org/10.1029/2007GC001604 (2007).
49. Andersen, M. B. *et al.* The tracing of riverine U in Arctic seawater with very precise ^{234}U/^{238}U measurements. *Earth Planet. Sci. Lett.* **259**, 171–185 (2007).
50. Thomas, A. L. *et al.* Penultimate deglacial sea-level timing from uranium/thorium dating of Tahitian corals. *Science* **324**, 1186–1189 (2009).

Author Contributions G.C., E.B. and B.H. were Principal Investigators for ODP proposal 519 designing this study. G.C. was co-chief scientist of IODP Expedition 310. P.D. and A.L.T. participated in the IODP sampling party. N.D., P.D. and A.L.T. performed U–Th dating of coral samples; N.D. performed X-ray diffraction analyses and reef growth modelling simulations; J.O. and Y.Y. performed geophysical modelling simulations; P.D. wrote the manuscript in collaboration with E.B. and B.H. The paper was refined by contributions from N.D., A.L.T., G.M.H. and G.C.

Author Information Reprints and permissions information is available at www.nature.com/reprints. The authors declare no competing financial interests. Readers are welcome to comment on the online version of this article at www.nature.com/nature. Correspondence and requests for materials should be addressed to P.D. (deschamps@cerege.fr).

.

The Tahiti records

Unlike islands located near active margins, such as Barbados or Vanuatu, Tahiti (Society Islands, French Polynesia) is a hot-spot volcanic island characterized by a slow and regular subsidence rate. Located at a considerable distance from large ice sheets, the coral reefs of Tahiti are far from major isostatic rebound effects, so that eustatic change dominates the local relative sea level (RSL) during deglaciation[27]. For this reason, the island of Tahiti provides an ideal far-field setting to constrain the Melt-Water Pulse (MWP) events that are thought to have punctuated the last deglaciation.

The first reconstruction of sea-level rise from Tahiti for the last deglaciation was established on the basis of two vertical holes (P6 and P7) drilled onshore through the modern barrier-reef in front of Papeete harbour[14]. Recently, this first record was augmented by three additional deviated holes (P8, P9, P10) at the same site[24]. In these onshore holes, the oldest age obtained for the last deglacial reef sequence (i.e. above the contact with Pleistocene reef carbonates) was 13.924 ± 0.064 ka BP (thousands of years Before Present, where Present refers to AD 1950) at 84.2 meters below sea level (mbsl). The absence of older material in these onshore holes is expected based on simple numerical model that simulates reef development in response to sea-level fluctuation. Such modelling demonstrates that the recovery of older deglacial corals, including those forming during the period spanning the Last-Glacial Maximum (LGM) and MWPs requires offshore drilling into the fossil reef structure seaward of the present-day barrier reef (see Bard et al.[14] or below).

The IODP Expedition 310 "Tahiti Sea Level"

The Integrated Ocean Drilling Program (IODP) Expedition 310 "Tahiti Sea Level" was carried out in October and November 2005. Logistical difficulties of working in shallow water required the utilization of a Mission Specific Platform, the *DP Hunter* vessel, equipped with a high specification dynamic positioning system allowing safe operation close to the coral reef. The offshore drilling operations recovered more than 400 m of post-glacial reef material[23] in three distinct areas around Tahiti (Fig. S1). Maraa and Faaa areas display a regular and gentle fore-reef slope from the outer edge to the modern barrier reef, while the Tiarei area exhibits two successive ridges on a depressed surface seaward of the living barrier reef. These ridges are invaluable features for sea-level reconstruction, because they allow us to document precisely the time window for MWP-1A (see main text for explanation).

In each of the three areas drilled during IODP 310, several boreholes were cored along transects at varying water depths (ranging from 41.6 to 117.5 m for the whole expedition) in an attempt to retrieve the entire postglacial reef sequence[23]. A total of 37 boreholes were drilled at 22 different sites, with penetration to a maximum depth of 161.8 mbsl. Standard core recovery was calculated at ~57%, but high-resolution downhole imagery and wire line logs indicate the presence of significant primary pore space such that the true recovery was actually much higher, and $> 90\%$[51].
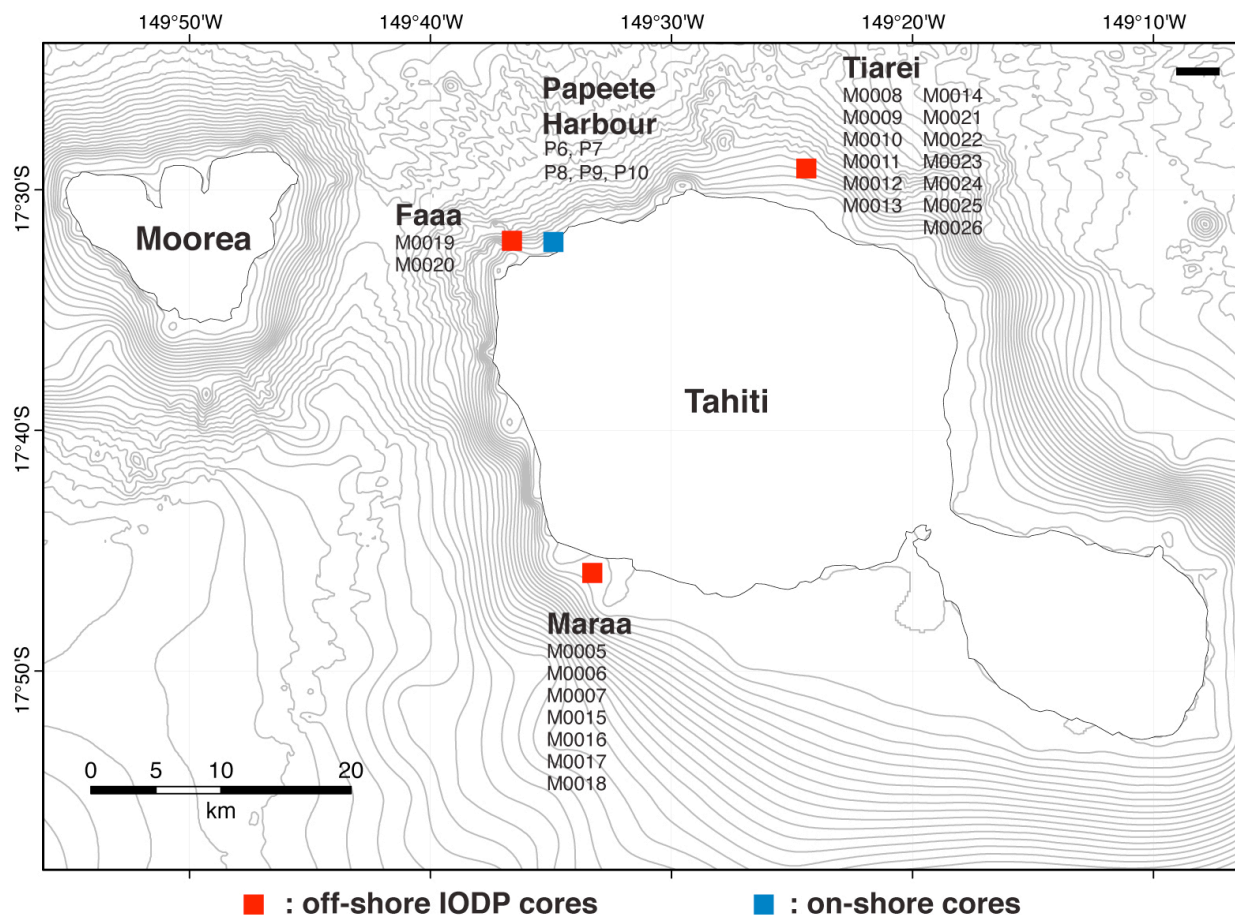
Figure S1: Location map of the three areas (Maraa, Faaa and Tiarei) investigated during Expedition 310 operations. For each area, the different sites cored are listed (from Camoin et al.[23]).

The reef framework that forms the bulk of the last deglacial carbonate sequence is characterized by the widespread development of microbialites, which locally represent the major structural and volumetric component of reef rock. Infilling of primary cavities by encrusting microbialites strengthens the coralgal frameworks, which contributed to the excellent core recovery achieved during Expedition 310. The excellent preservation of the original framework also offers reliable evidence as to which samples are in growth position when sampling for sea-level reconstruction.

In several cases, we also dated coral samples that belong to the unconsolidated horizon occurring at the base of the deglacial sequence. Although there is, in at least some cases, no clear evidence for *in situ* position, these samples can nevertheless be of significant interest because they constitute the first datable material of the post-glacial reef sequence in each drill hole and, therefore, may provide insights into the timing of reef initiation on the submerged surface of older Pleistocene reef carbonates.

Although we dated various types of corals (see Table S2), U-Th dating were mainly focused on massive *Porites* (mp), robust branching *Pocillopora* (rbp) and branching *Pocillopora* (bpo). These genera are abundant in offshore holes and, in most cases, are free of encrusting microbiallites; they could therefore be easily

cleaned prior to dissolution and represented the most suitable material for U-Th dating. We also determined the ecological assemblages to which the coral samples belong (Table S2) on the basis of the six distinctive coralgal assemblages previously identified in the IODP holes[52-54]:

1. the robust branching *Pocillopora*/massive *Montipora* (PM) assemblage, indicative of the shallowest water depth of 0 to 10 m;
2. the massive *Porites* (mP) assemblage that thrives at depths ranging from 0 to 20 m, and is occasionally seen at depths up to 25 m;
3. the tabular *Acropora* (tA) assemblage that thrives at depths ranging from 5 to 15 m;
4. the branching *Porites*/*Pocillopora* (PP) assemblage that also thrives at depths ranging from 5 to 15 m;
5. the branching *Porites*/encrusting *Porites* and *Montipora* (PPM) assemblage that characterizes somewhat deeper environments (5 - 25 m);
6. the encrusting *Agaricid* and *Faviid* (AFM) assemblage that typifies environments deeper than 20 m.

Occurrence of vermetid gastropods that are indicative of shallow environments (< 5 - 6 m)[25] was also noted in some samples as a robust water-depth indicator.

Noteworthy is the scarcity, in offshore holes, of the robust branching *Acropora* gr. *robusta-danai* species. This species typifies the "APH" assemblages (Acropora robusta/danai and Pocillopora cf. verrucosa and thick crusts of Hydrolithon onkodes)[55,56] that prevails in onshore drill holes, especially after 12 ka BP[14,55,57]. In IODP holes, robust branching *Acropora* are very rare in the Faaa and Maraa reef sequences prior to ~13.9 ka BP, and are totally absent in the Tiarei sequence. The striking appearance of *Acropora* gr. *robusta-danai* as a dominant species in the Tahiti reef, coeval with the end of MWP-1A, may be related to a significant change in environmental conditions concurrent with the MWP-1A event. The ecological implications of this finding will be discussed elsewhere[54].

[230]Th-U dating of coral: analytical procedures and results

U-Th analyses are reported in Table S2. Activity ratios and ages are calculated using the decay constants determined by Cheng et al.[58]. All reported errors are given at the 2σ level. Labels (#1, #2, …) indicate replicate analyses obtained on different pieces of the same coral sample. U-Th ages are calculated using the Isoplot software[59]. No correction for detrital [230]Th were processed because [232]Th concentrations are in most cases low (≤ 0.5 ppb). Ages are presented in years before 1950 AD.

XRD detection of secondary calcite in corals

For each coral sample, we checked the presence of diagenetic calcite by powder XRD analysis. We used a calibration method optimized for the detection and quantification of very low amount of secondary calcite. The procedure, described in detail in Sepulcre et al.[60], relies on a thorough calibration of the instrument by means of gravimetric pure standard mixtures and was assessed using two different XRD instruments. It is worth mentioning that this procedure involves measuring XRD peak areas rather than peak heights alone. Reproducibility tests convincingly demonstrate that this is the optimal method for precise quantification of calcite when it constitutes

a small fraction of the total mass. To take into account possible natural heterogeneity in the coral samples, XRD determinations were carried out on three distinct slides for each sample. Detection limit for calcite achieved by this method is about 0.2%[60]. Quantification limit[61] is about 0.9%. This last theoretical quantification limit does not reflect the true overall analytical performance; standard measurements demonstrate that quantification is possible at 0.3% calcite. Only samples that contain < 1% calcite were considered for U-Th dating in this paper. This criterion follows that used in previous work[62,63].

U-Th analyses

Most U-Th analyses were performed using a VG-54 thermo-ionisation mass spectrometer equipped with a 30 cm electrostatic analyzer and a pulse-counting Daly detector at the CEREGE. We prepared a mixed ^{233}U-^{236}U-^{229}Th spike that was calibrated against the Harwell HU-1 uraninite standard (using an aliquot of the solution originating from GEOTOP). For the calibration of the $^{229}Th/^{233}U$ ratio, we adopted the $^{230}Th/^{238}U$ mean atomic ratio for HU-1 determined by Cheng et al.[58] for this solution (19.995×10^{-6}), which deviates by 3‰ from the secular equilibrium value (19.939×10^{-6}). The $^{236}U/^{233}U$ spike ratio (~1) was calibrated against the $^{238}U/^{235}U$ ratio of the HU-1 solution, assuming a value of 137.88, following the procedure described in Deschamps et al.[64]. Recent measurements have demonstrated that this ratio is not completely homogenous in nature (e.g. Stirling et al.[65] or Weyer et al.[66]), and have indicated a value in HU-1 of $137.769 \pm 0.011/0.024$[67]. Here, however, we maintain the use of the previously assumed value of 137.88 to ensure that calculated ages can be directly compared to previous data from Tahiti. The < 1‰ difference in assumed and measured $^{238}U/^{235}U$ values in HU-1 leads to an insignificant change in final ages. Stirling et al.[65] have also evaluated the impact of variations in $^{238}U/^{235}U$ on the accuracy of U-series ages. They calculated the bias in U-series isotopic compositions and age resulting from a departure of the $^{235}U/^{238}U$ ratio away from 137.88 for different analytical configurations (e.g. ^{233}U-^{229}Th or ^{236}U-^{229}Th spikes). Although they did not explicitly explore the present case where the mass discrimination is internally monitored by a $^{236}U/^{233}U$ spike, they showed that only minor offsets in age (few years) and $(^{234}U/^{238}U)_0$ will be induced for young samples (< 30 ka), especially when the HU-1 standard solution is used to calibrate the spike tracer. It is also noteworthy that, according to Stirling and co-authors, the $^{238}U/^{235}U$ isotopic compositions of seawater and marine carbonates are identical within analytical uncertainties to that of the HU-1 standard. Thus, our analytical approach likely cancels out any systematic offset due to a departure from the accepted $^{238}U/^{235}U$ value for marine samples.

The U-concentration of our mixed spike was calibrated against the NIST-SRM4321B standard solution, with a certified U-content and an overall 2σ uncertainty of about 6‰ (*i.e.* larger than the individual statistical errors on TIMS U-content analyses). Our spike calibration was assessed by comparison with a mixed gravimetric $^{238}U/^{232}Th$ standard and yielded results consistent with those obtained with a previous ^{233}U-^{229}Th spike used at CEREGE.

For uranium analyses, masses 233, 234, 235 and 236 are measured in peak jumping mode. The $^{236}U/^{233}U$ ratio is used to monitor internally the instrumental mass bias effects. This strategy avoids monitoring the large ^{238}U ion beam, and avoids many of the problems related to gain calibration of the Daly/Faraday detectors[64,65]. For thorium analyses, techniques are similar to those reported previously[68].

The long-term reproducibility of U-isotope analyses achieved during the course of this study was assessed by replicate measurements on the NBS-960 international standard and yielded a mean value of $(^{234}U/^{238}U) = 0.9635 \pm 0.0008$ (2σ, n = 23) in excellent agreement with our previous determinations of the same standard: $(^{234}U/^{238}U) = 0.9634 \pm 0.0037$ (2σ, n = 6)[14] and $(^{234}U/^{238}U) = 0.9624 \pm 0.0019$ (2σ, n = 23)[69] and with values reported in the literature see determinations and compilation by Deschamps et al.[64] and Andersen et al.[70]. The 2σ precision of U-Th ages ranges in most cases from 1.5 to 4‰ ($\pm$ 20 to 50 years in ages). Internal reproducibility was also checked by replicate measurements of several samples that all show agreement within errors (Table S2).

Calculated initial $(^{234}U/^{238}U)_0$ values of post-glacial samples analysed in this study yield a mean value of 1.1458 ± 0.0020 (2σ). This value is consistent with recent determinations of modern sea water and corals[69,71,72]. For coeval corals, $(^{234}U/^{238}U)_0$ values agree within analytical reproducibility. This clustering of $(^{234}U/^{238}U)_0$ values (Table S2) substantially narrows the uncertainties in marine $(^{234}U/^{238}U)_0$ value compared to previous datasets (e.g. Vanuatu, Papua New Guinea and Barbados) that encompass this period[29,72,73] and is significantly narrower than the $\pm$ 4.8‰ range adopted by the IntCal Working Group et al.[30,62] for the interval 0-17 ka.

Some samples were also analysed at Oxford using a MC-ICP-MS (see detailed analytical procedure in Thomas et al.[50] and Mason and Henderson[74]. In order to assess the external reproducibility, duplicate measurements were also performed by the Oxford team and CEREGE team, which also showed very good agreement (see Table S2).

Subsidence rate of Tahiti

The Tahiti Island is part of the Society archipelago formed as the Pacific plate drifted over a fixed hot spot. It is thus characterized by a slow and regular subsidence. A long-term (1 Ma) subsidence rate has been estimated at about 0.25 mm/yr[75] while a value of 0.15 mm/yr has been reported for the Holocene[76]. This value is compatible with the lower estimate of 0.2 mm/yr based on the recovery of an aerial basalt lava flow, dated at 549 ± 11 ka (2σ) by K-Ar, at ~ 114 m depth below the carbonate sequence in the P7 onshore hole[14].

Data obtained on pre-LGM Tahiti corals[50,77] that provide absolute maximum constraint on subsidence, over the past 325 ka, are consistent with this first estimate of 0.25 mm/yr. Two corals collected at 147 mbsl with U-Th ages of 153 ka (MIS 6) indicate an upper limit of 0.4 mm/yr for the subsidence of the island, assuming a MIS 6 sea-level lowstand of < 90 m. Corals of MIS 9 age provide also a maximum constraint on subsidence rate of 0.39 ± 0.03 mm/yr, assuming that sea level during MIS 9 was similar to that of todays. It is noteworthy that it is very likely to have been lower, allowing for the depth of water that the corals grew under, and for the possibility that they did not grow at the sea level maximum[77].

Modern subsidence was recently assessed by Fadil et al.[78] with direct measurements by GPS and other geodetic instruments. These authors calculated an arithmetic average rate of 0.5 mm/yr based on four Tahiti GPS stations (0.25 ± 0.5, 0.3 ± 0.6, 0.6 ± 1.6, 0.8 ± 0.8 mm/yr). Taking into account the uncertainty for each value leads to a weighted average of 0.38 ± 0.34 mm/yr. In their Table 3, Fadil et al.[78] also listed three other modern subsidence values based on geodetic approaches

(0.04 ± 0.2, 0.27 ± 1.1, 0.2 ± 0.3 mm/yr). A weighted average of 0.15 ± 0.15 mm/yr can be derived by using all seven values provided by Fadil et al.[78] for the modern subsidence rate.

Consequently, the various subsidence estimates, obtained by different methods over different time scales, are in agreement with the value of 0.25 mm/yr, chosen for our work and previously used by Bard et al.[14,24]. We can further assume that the true value lies within a range between a minimum value of 0.2 mm/yr (based on K-Ar of aerial basalt in a Tahiti core) and a maximum value of 0.4 mm/yr (based on older Tahiti corals, Thomas et al.[50,77]). The maximum systematic difference in corrected bathymetry is thus ca. 3 meters for a 16 ka coral. Consequently, the subsidence uncertainty is always smaller than the error linked to the limited knowledge on the depth habitat of individual coral species. It is also important to assess the possible impact of subsidence variations during the MWP-1A time window which lasted 350 yr. A temporal variation within the 0.2 - 0.4 mm/yr range would alter the relative position of corals by less than 10 cm, hence completely negligible in the frame of our scientific discussion. This difference would remain less than 20 cm even by assuming that the instantaneous subsidence had varied between extreme values of 0 and 0.5 mm/yr.

The extended Tahiti record and the Timing and Amplitude of MWP-1A event

The deglacial Tahiti record is now based by more than 200 U-Th age data. For samples collected during the IODP expedition, in almost each hole, all ages are in stratigraphic order (see Fig. S2) substantiating the reproducibility of the analytical method and the overall excellent preservation of the corals collected during offshore coring.

The general MWP-1A features rely on critical samples that belong to coral sequences in holes M0023A, M0023B, M0024A and M0015A. These sequences are central to assessment of the MWP-1A event and are described in detail in Figure S3.

Sea level during the early part of the deglaciation

The oldest sample (9B-15R-1W 13-20) retrieved in the deglacial sequence during the IODP Expedition is dated at 16.09 ± 0.04 ka BP (see Fig. S4). This robust branching *Pocillopora* was collected at a subsidence-corrected depth of 117 mbsl, at the interface with the underlying Pleistocene unit. The sample is in growth position and belongs to the shallow-water coralgal assemblage *Pocillopora*/massive *Montipora* (hereafter "PM assemblage") that typifies the shallowest depositional environment at depths less than 10 m at Tahiti. This sample constrains the RSL to the 117 - 107 m range during the first part of the deglaciation. Although it is a reworked clast, the robust branching *Pocillopora* (24A-15R-1W 16-20) collected at a corrected depth of 115 mbsl and dated at 15.74 ± 0.03 ka strengthens this first estimate. Further constraints are provided by an encrusting *Montipora* (25B-11R-1W 70-74) collected at a subsidence-corrected depth of 114 mbsl. This sample, dated at 15.31 ± 0.02 ka BP, is associated with vermetid gastropods whose bathymetric habitat is restricted to less than ~5 m depth[25,57,79]. This constrains RSL to 114 - 109 mbsl at 15.31 ka (Fig. S4). Assuming that the sea level did not drop during that period, we may infer that sea level was between 117 and 109 mbsl during the early part of the deglaciation (~16 ka) at Tahiti.
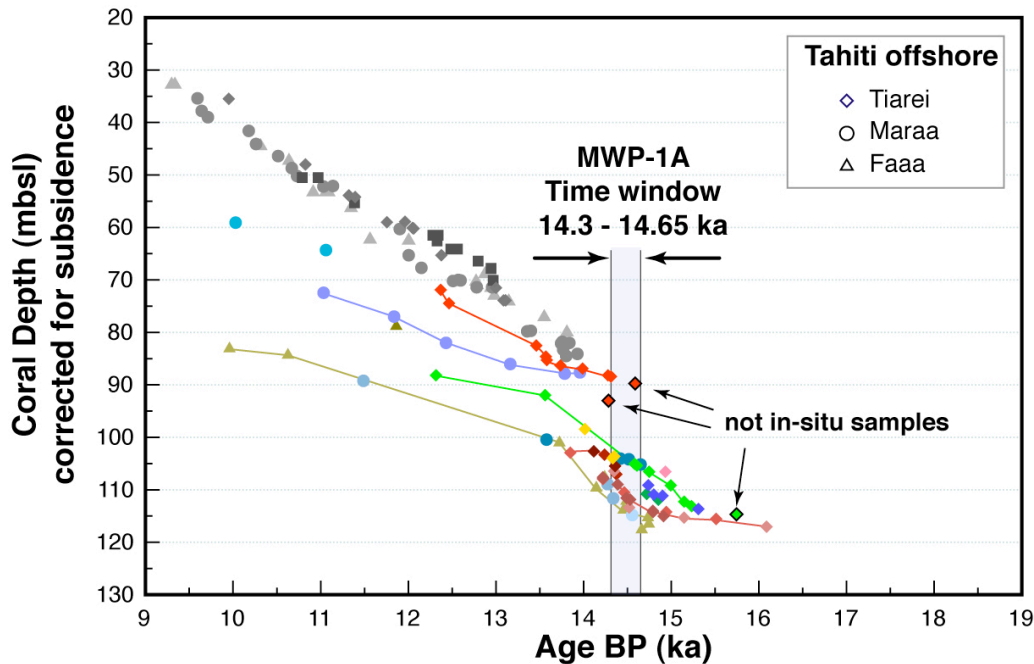
Figure S2: Sea-level history reconstructed from onshore and offshore holes drilled in the Tahiti coral reef. Onshore holes are represented by grey symbols whereas holes drilled during the IODP Expedition 310 "Tahiti Sea Level" and reported here for the first time are represented by coloured symbols. Lines are drawn between points from the same hole to show that samples are in correct stratigraphic order. Samples that are not in situ are highlighted with arrows. Ex-situ samples from holes M0023A&B could indicate that MWP-1A ended before 14.31 ka BP.

Pre-MWP-1A sea level

The pre-MWP-1A sea level is constrained by three samples collected at a subsidence-corrected depth of 105 mbsl (see Fig. S4): two robust branching *Pocillopora* (samples 24A-10R-1W 65-75 and 24A-10R-1W 98-116, see Fig. S3-a) and one massive *Montipora* (15A-37R-1W 19-28). The latter sample is in growth position and grew immediately on pre-glacial substratum (Fig. S3-b). The two Robust Branching *Pocillopora* belong to the shallow-water coralalgal assemblage PM (< 10 m). These samples are also associated with vermetid gastropods that are indicative of a very shallow environment < ~5 m[25,57]. Based on these shallow-water coral samples, we consider that we can realistically constrain sea level to 105 - 100 mbsl between 14.65 - 14.60 ka.

We propose that this range should be restricted further to 104 - 100 mbsl, by considering that these coral colonies grew most likely at least 1 meter below the mean sea level. This is substantiated by the position of the two samples found at shallowest depths in holes M0024A and M0011A prior to MWP-1A: a robust/columnar *Porites* (24A-10R-2W 69-72) and a massive *Porites* (11A-6R-1W 24-35) that were both living at a depth of 106.5 mbsl and dated at 14.75 ± 0.03 ka and 14.93 ± 0.06 ka, respectively (Fig. S4). The assumption of a nonzero sea-level rise (on the order of at least 10 millimetres per year, a rate that seems realistic for this time window since the mean rate estimated for the early part of the last deglaciation is 11.1 ± 2.4 mm/yr - see Section "Rate of sea-level rise"-) implies that the sea level reached at least 104 mbsl at 14.65 ka (2.5 m rise in 250 years).
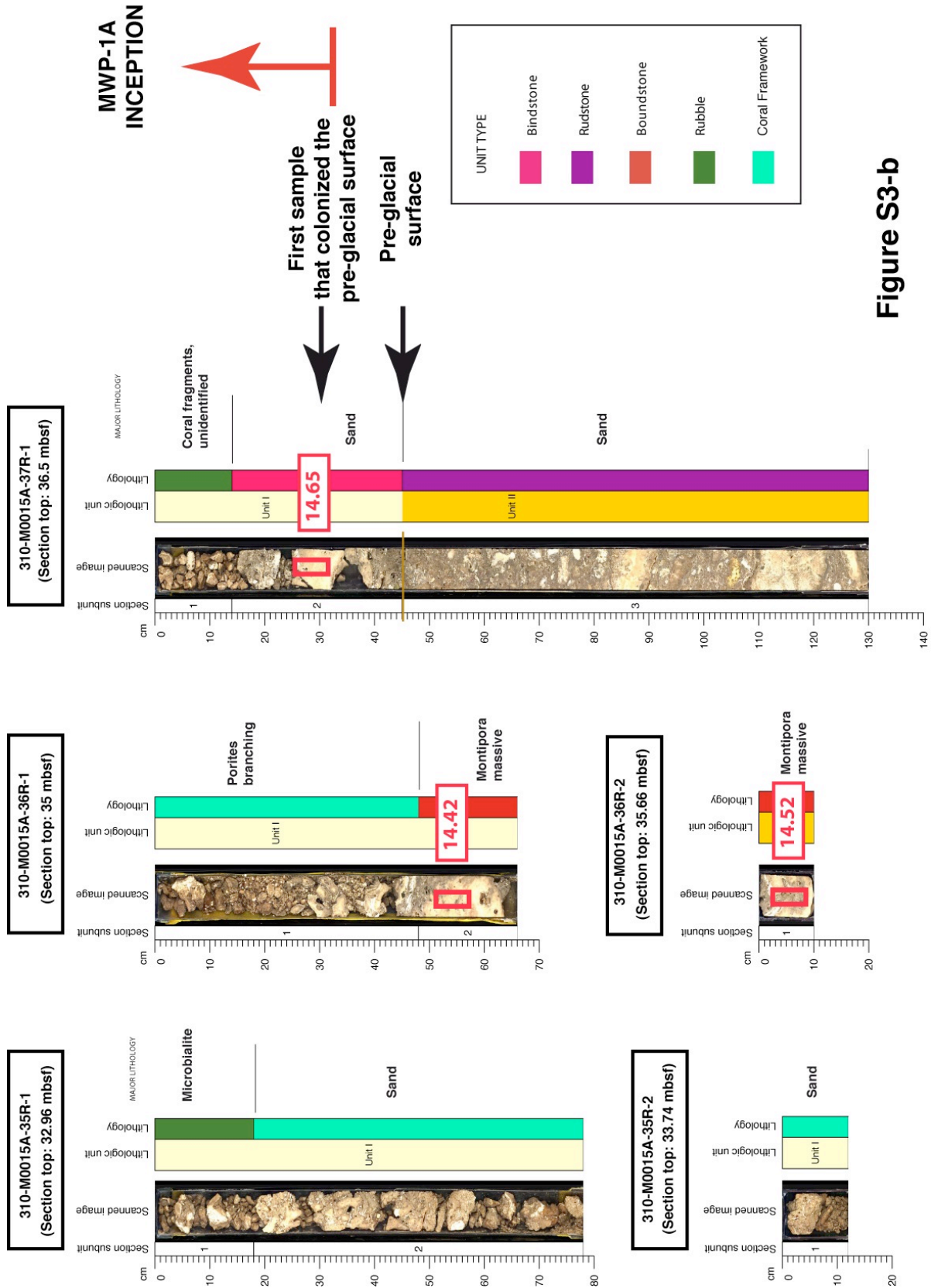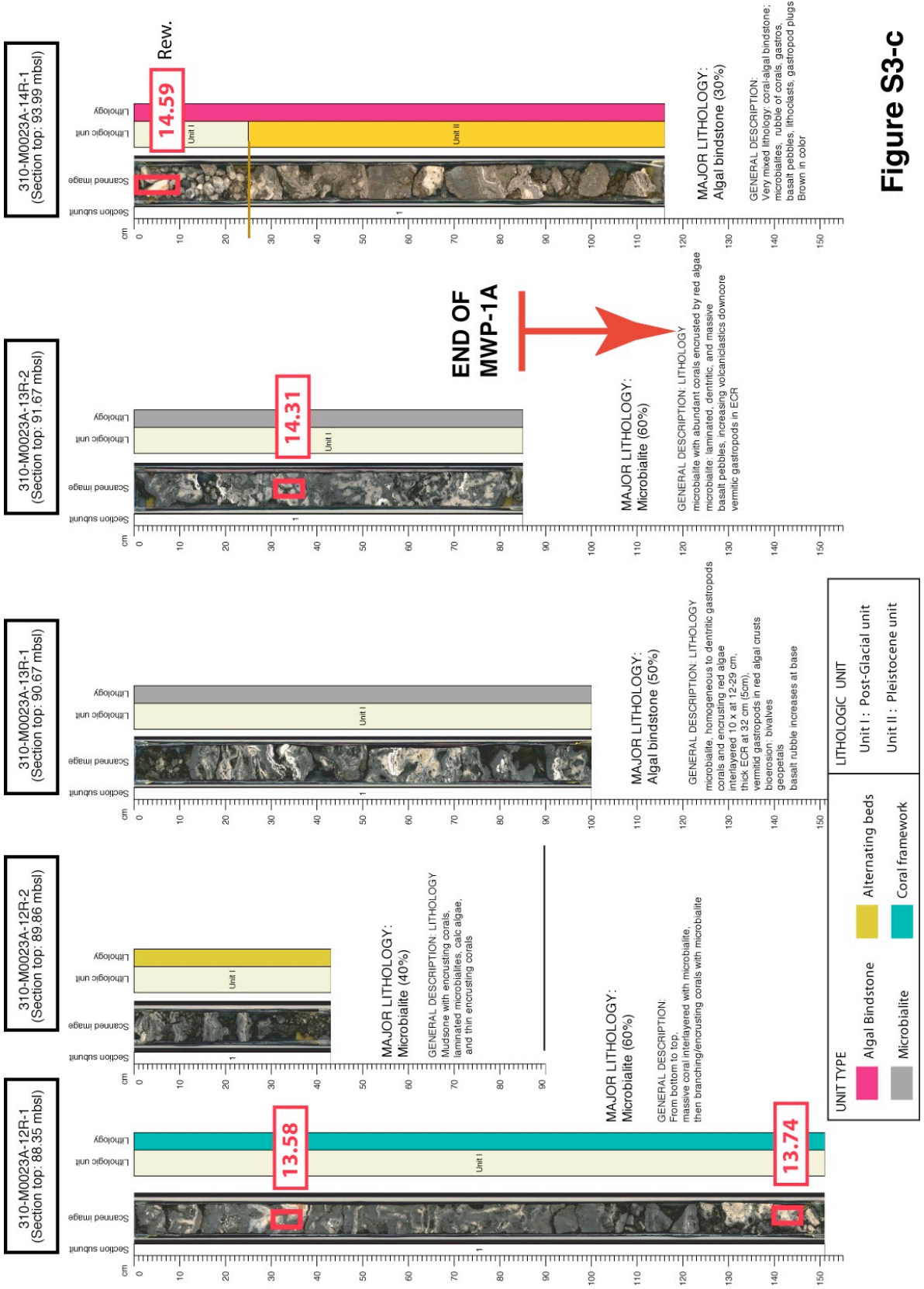
Figure S3-a

Figure S3-b

Figure S3-c

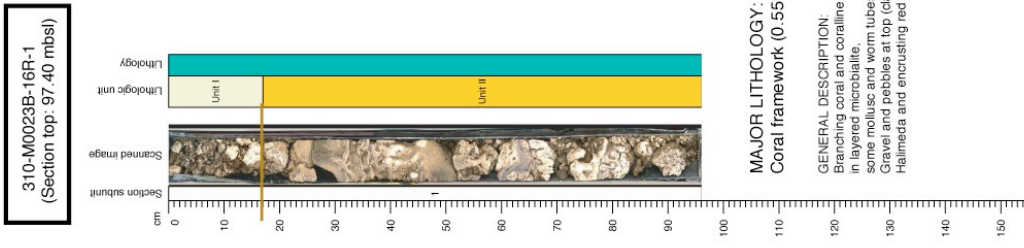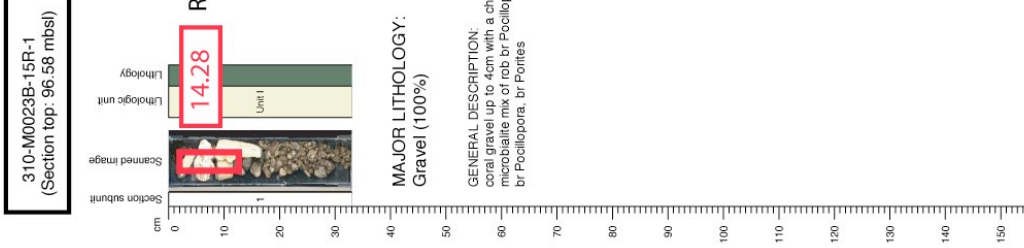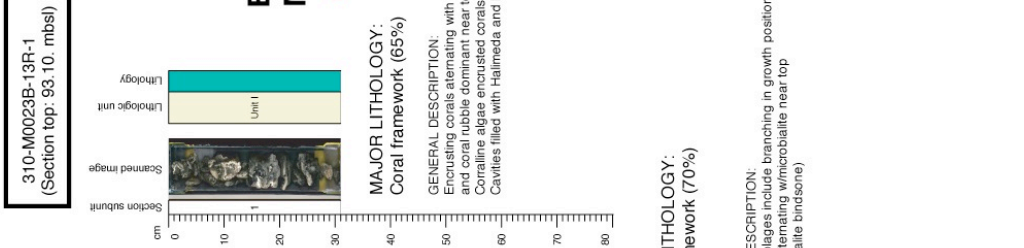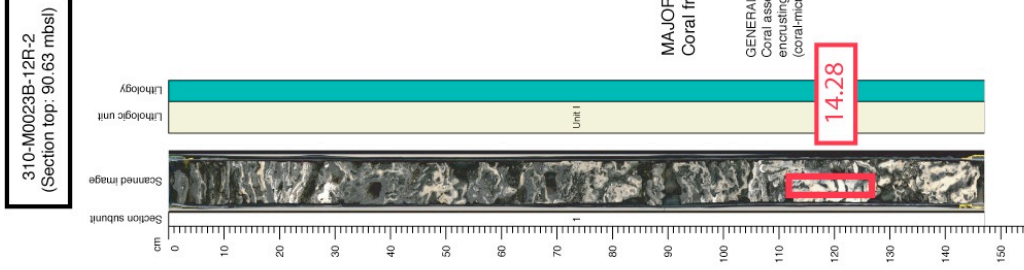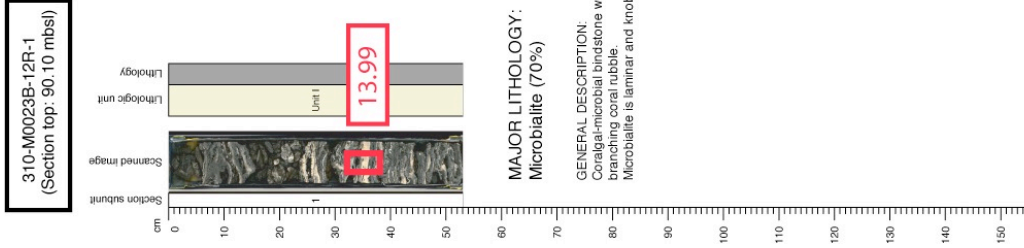Figure S3-d

Figure S3: Lithological description of key coral sequences that portray the MWP-1A event. Ages are U-Th dating in ka before 1950 (Table S2). Fig. S3-a: Line scans of core sections 9R-1 – 10R-1 from Hole M0024A (Tiarei). Fig. S3-b: Line scans of core sections 35R-1 – 37R-1 from Hole M0015A (Maraa). Fig. S3-c: Line scans of core sections 12R-1 – 14R-1 from Hole M0023A (Tiarei). Fig. S3-d: Line scans of core sections 12R-1 – 16R-1 from Hole M0023B (Tiarei). Adapted from Camoin et al.[23].

In addition to the shallowest coralgal assemblages discussed above, we also dated a number of deeper-living coral samples, that were living up to 118 mbsl (subsidence corrected) during the same time window, clearly deeper than the estimated sea level (see Fig. S4). In general, this depth range is consistent with the modern depth distribution of those species (Fig. S4). However, a noticeable exception is the Robust Branching *Acropora* sample 20A-24R-2W 38-42 (Faaa site) dated at 14.66 ± 0.06 ka. This sample is accompanied by Robust Branching *Pocillopora* and Encrusting *Montipora*[23], an assemblage that generally typifies a shallow environment. By analogy with its modern counterpart, the depth interval of this assemblage is generally less than 10 m[25] and it seems statistically unlikely that this coral assemblage could have thrived at depths reaching 20 m. In this case, the sample was at least at 14 m below sea level at that time (i.e. the difference between its depth of 118 m and other species found at 104 m; see Fig. S4). We hypothesize that this can be considered as an indication that sea level was probably in the lower half of the conservative range deduced above, which would suggest a pre-MWP-1A sea level of ≈ 104 - 102 m in the 14.65 - 14.60 ka time window.

Timing of MWP-1A inception

Determining with accuracy the MWP-1A inception remains challenging, but it is very likely that the uppermost limit for the onset of the melting is marked by the three samples 24A-10R-1W 65-75, 24A-10R-1W 98-116 and 15A-37R-1W 19-28, dated at 14.58 ± 0.05 ka, 14.61 ± 0.03 ka and 14.65 ± 0.02 ka respectively. As discussed in the main text, bracketing more precisely MWP-1A inception (i.e. at a decadal scale) requires taking the reef response to acceleration in sea-level rise into account (i.e. the time interval during which a particular coralgal assemblage remains within its depth tolerance; note that this is completely different to the time lag required to colonize the Pleistocene surface after its flooding). This is illustrated in Fig. S4b which shows that the two robust branching *Pocillopora* samples dated at 14.58 and 14.61 ka may have accommodated the first part of the sea-level rise related to MWP-1A. Assuming a local rate of sea-level rise on the order of 50 mm/yr during MWP-1A and considering that these two coral colonies may have grown 5 meters beneath the sea surface, the inception of MWP-1A may have started 100 years earlier. Considering our preferred range of 104 - 102 mbsl, this pushes the MWP-1A inception earlier by ca. 50 years. For these reasons, we consider that the earliest possible age for MWP-1A inception is 14.65 ka. A similar logic was used by Liu and Milliman[33] in their revisitation of the Barbados MWP-1A chronology.

It is however possible that MWP-1A may started significantly later, as young as 14.5 ka, as potentially marked by sample 15A-36R-2W 0-6 from hole M0015A dated at 14.52 ± 0.02 ka (see Fig. S3-b and the "extreme" scenario in Fig. S4-b).
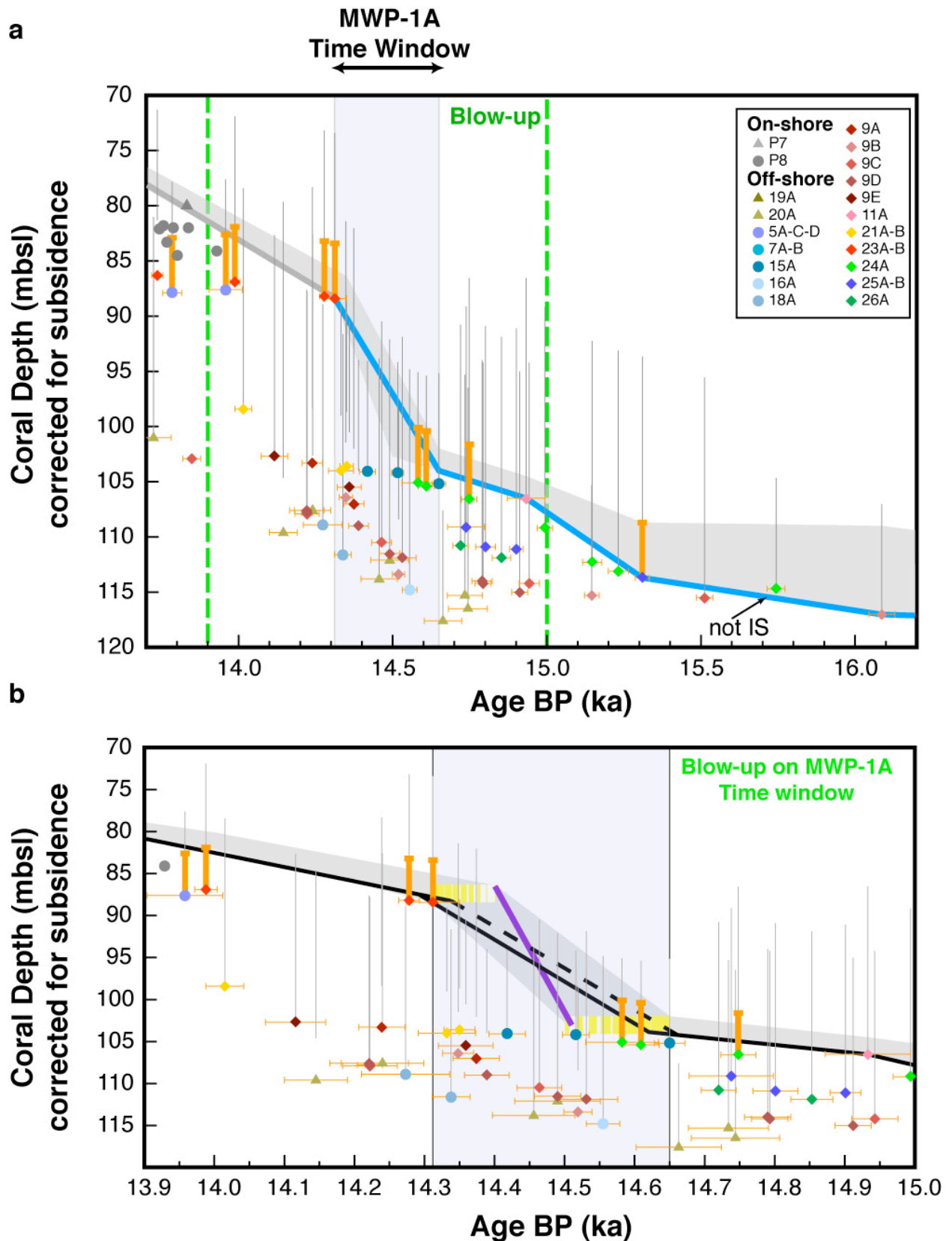
Figure S4: The deglacial Tahiti sea-level record. (a) Coral core depths vs U-Th ages of Tahiti samples for the 16.2 - 13.7 ka time window. Grey symbols correspond to coral samples collected in onshore holes[24], whereas coloured symbols correspond to in situ samples collected in offshore holes drilled during the IODP Expedition 310 reported here for the first

time. Depths are expressed in meters below present sea level and are corrected for a constant subsidence rate of 0.25 mm/yr. Error bars reported for U-Th ages are 2σ. The vertical bars reported for each coral sample correspond to their optimal bathymetric habitat range inferred from the coralgal assemblage identification: 0 - 10 m for PM assemblage, 0 - 20 m for mP, 5 - 15 m for tA and PP assemblages, 5 - 25 m for PPM assemblages. For the AFM assemblage (> 20 m), no vertical bar is displayed. Orange bars indicate samples associated to vermetid gastropods that are indicative of shallow environment (0 - 5 m). The blue line delineates the sea-level curve obtained by considering the tie points previously determined by Bard et al.[24] for the 0 - 14 ka period and those discussed in the text after that period (Table S1). In this scenario, MWP-1A event lasted 350 ka and had a ~16 m amplitude. The shaded grey band illustrates our estimate of the most likely range of the Tahiti RSL over the last deglaciation. It is constrained by considering the lower (blue line) and upper bounds of sea-level changes constrained by taking the ecological ranges of multiple coralgal assemblages. For the tie points previously defined by Bard et al.[24], a reasonable leeway of 2 m was considered. For the MWP-1A time window, this estimate takes into consideration that the MWP-1A event might start later than 14.65 ka and end earlier than 14.31 ka.

(b) Blow-up of the MWP-1A time window (15 - 13.9 ka). The two yellow areas represent the most realistic range that we infer for the MWP-1A onset and termination in terms of timing and sea level (see text). The shaded grey band illustrates our estimate of the most likely range of the Tahiti RSL over the last deglaciation as in Fig. S4-b. The purple line represents an extreme, but possible scenario involving a very abrupt MWP-1A event that started at 14.5 ka and finished at 14.4 ka with an amplitude of 18 meters. The black broken line represents a plausible scenario involving a rate of sea-level rise of 50 mm/yr during MWP-1A and considering that the sea level attained 104 mbsl (the upper bound of our preferred range) at the time that the two Pocillopora samples dated at 14.58 ka and 14.61 ka grew. This scenario shows that the MWP-1A inception may have started at 14.65 ka. Another scenario (dashed black line) still assumes a 50 mm/yr rate of sea-level rise but considers that the two branching Pocillopora lived ca. 5 meters beneath sea surface. In this case, the MWP-1A inception may have started 100 years earlier.

Reef response to MWP-1A

The change in reef development strategy that follows the MWP-1A is well documented in hole M0024A where shallow-water assemblages dominated by robust branching *Pocillopora*, massive *Porites* and encrusting *Montipora* were substituted for branching *Porites* species after 14.58 ka (see Fig. S3-a). These branching *Porites* belong to the branching *Porites/Pocillopora* (PP) assemblage which is typical of an environment of moderate energy and light intensity, ranging from 5 to 15 m depth.

Investigations of Site M0009 (Tiarei) samples provide further evidence of such an ecological response to MWP-1A. At this site, we observe a rapid increase in the

vertical accretion rate of the reef accompanied by a change in coralgal assemblages (see Fig. S5), from the shallowest assemblage (PM) to the deepest assemblages (AFM, PPM). This occurred at 14.5 ka. Although this cannot be regarded as a definite demonstration, we argue that this increase in the vertical accretion rate probably occurred in response to the sea-level rise related to MWP-1A.
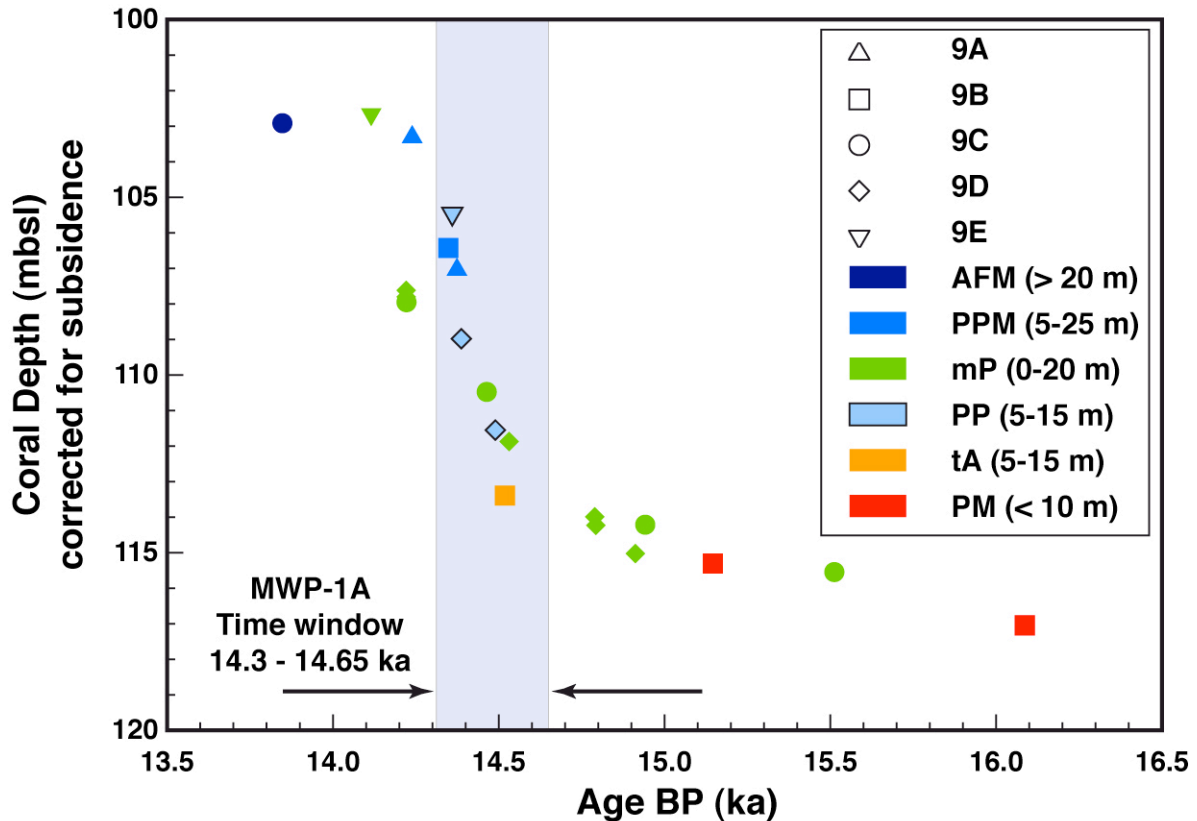
Figure S5: Increase in vertical reef accretion rate of the reef at Site M0009 (Tiarei) in response to the acceleration in sea-level rise related to MWP-1A. The reef response is accompanied by a change in coralgal assemblages (PM: robust branching Pocillopora/massive Montipora; tA: tabular Acropora; mP: massive Porites; PP: branching Porites/Pocillopora; PPM: branching Porites/encrusting Porites and Montipora; AFM: encrusting agaricids and faviids).

MWP-1A termination and post-MWP-1A sea level

The end of MWP-1A is evidenced by a discontinuity within the sedimentary record and is captured by shallow coral samples recovered at the interface of the underlying Pleistocene in holes drilled at an intermediate position on the fore-reef slopes of Tiarei sites. The coral samples that marked the MWP-1A termination were recovered in holes M0023A (Fig. S3-c) and M0023B (Fig. S3-d). In these holes, the first datable corals to colonize the pre-glacial substratum after the sea-level jump are two branching *Pocillopora*. These two samples are in growth position and are dated at 14.28 ± 0.02 ka (23B-12R-2W 113-127) and 14.31 ± 0.04 ka (23A-13R-2W 32-37). These samples provide a robust constraint on the end of the MWP-1A event at ~14.31 ka. This can be considered a lower bound for the MWP-1A chronozone if we take into account the time lag in reef initiation (i.e. the time required by corals to

colonize the Pleistocene surface that followed substrate flooding). Two reworked coral fragments recovered at the interface of the underlying Pleistocene unit in cores 23A-14R and 23B-15R are dated at 14.59 ± 0.03 ka and 14.28 ± 0.03 ka respectively (see Fig. S3-c, S3-d and Fig. S2). Although these samples should be interpreted with caution because they were not in-situ, they might indicate that the end of MWP-1A was older than 14.3 ka (Fig. S2).

The two *in situ* branching *Pocillopora* samples were recovered at a subsidence-corrected depth of 88 m. They belong to a coralgal assemblage that is indicative of shallow-water conditions (< 15 m) and are also associated with vermetid gastropods. This constrains the paleodepth range to ≤ 5 m[25] and provides a first conservative estimate (i.e. 88 - 83 mbsl) of the sea level at 14.31 ka at Tahiti. These first constraints seem robust because a sea level above 83 mbsl at 14.31 ka would imply sea-level rise close to zero for the next 300 years, (onshore data - P7 and P8 holes - indicate a sea level near ~80 mbsl at 14 ka; see Fig. S5 and Bard et al.[14,24]). Note also that we cannot rule out that these corals grew just below the surface of the water, 88 m is thus a plausible lower bound for the post-MWP-1A sea level.

As discussed above for the pre-MWP-1A sea level, we must also take into consideration the coral colonies that thrived between 112 - 103 mbsl during the 14.4 - 14.2 ka time window (see Fig. S4b). During the 14.3 - 14.2 ka interval (i.e., after MWP-1A termination), most of the corals that we dated are massive *Porites* (18A-18R-1W 40-50, 109 m depth; 18A-19R-1W 107-110, 112 m depth; 9C-11R-2W 0-4, 108 m depth; 9D-7R-1W 11-28, 108 m depth; 9D-7R-1W 28-45, 108 m depth). Abbey et al.[53] have identified these Massive *Porites* as *P. lobata* (holes M0018A and M0009D) and *P. solida* (hole M0009D), which are abundant up to 20 m water depth and may be observed up to 25 m deep in modern reef systems from French Polynesia[25,54,80-85]. Several branching *Pocillopora* or *Porites* (9D-7R-2W 64-71; 9E-9R-1W 32-36; 21A-17R-1W 13-19; 21B-16R-1W 39-44) are also observed between 109 and 104 mbsl during the 14.4 - 14.3 ka time span, i.e. just before or during the MWP-1A termination. These corals belong to the PP coralgal assemblage that generally developed at depths ranging from 5 to 15 m[54]. It is remarkable that most of these samples are either in the deepest part of their usually accepted habitat depth range, or even deeper than this range by several meters (Fig. S4). Therefore, we consider again that this gives us a clue that sea level was most likely close to the lower-end limit of the 88 - 83 m conservative range derived from the shallowest coral specimens. Assuming again that sea level was probably within the lower half of this range, this would therefore lead to a reduced estimate of ca. 88 - 86 m after the MWP-1A termination.

MWP-1A amplitude

Considering the most conservative estimates discussed above for the pre- and post-MWP-1A sea-level positions (i.e. 105 - 100 mbsl and 88 - 83 mbsl), we derive a MWP-1A amplitude ranging from 12 to 22 meters. Based on arguments above, however, we consider it more likely that the true amplitude was between 14 and 18 meters (104 - 102 mbsl and 88 - 86 mbsl). In either case, the middle of the amplitude range is 16 or 17 meters.

We are fully aware of the uncertainties related to the sea-level determinations using habitat zone of different coral species, which often have only a limited statistical

significance. Accordingly, we also consider an alternative approach to constrain the MWP-1a amplitude at Tahiti, which follows Bard et al.[24] who determined average rates of sea-level rise around the Younger Dryas period. We calculate mean local rate of sea-level rise throughout the pre- and post-MWP-1A periods by means of linear regression fitted through the uppermost samples for the periods before and after the jump (see Fig. S6). For the post-MWP-1A period (i.e. 14.31 ka to 12.85 ka), we include the two branching *Pocillopora* samples (23B-12R-2W 113-127; 23A-13R-2W 32-37) from site M0023 that mark the end of MWP-1A, together with all onshore samples, with the exception of those of the lower part of the P8 hole (as discussed in Bard et al.[24]). We calculate a mean rate of 13.8 ± 1.1 mm/yr (2 standard errors). For the pre-MWP-1A period, we take into consideration all the uppermost samples in the holes from the 16.2 to 14.6 ka time window (see Fig. S6). For this period, we obtain a mean rate of 11.1 ± 2.4 mm/yr. The MWP-1A amplitude at Tahiti can be assessed by considering the gap between the two linear fits. Using this approach, we deduce a MWP-1A amplitude of 17 meters with a 2 σ uncertainty of 2.2 meters (estimated by considering the error envelope on linear fits -see Fig S6). This value agrees closely with the estimate inferred from the depth distribution of coralgal assemblages.
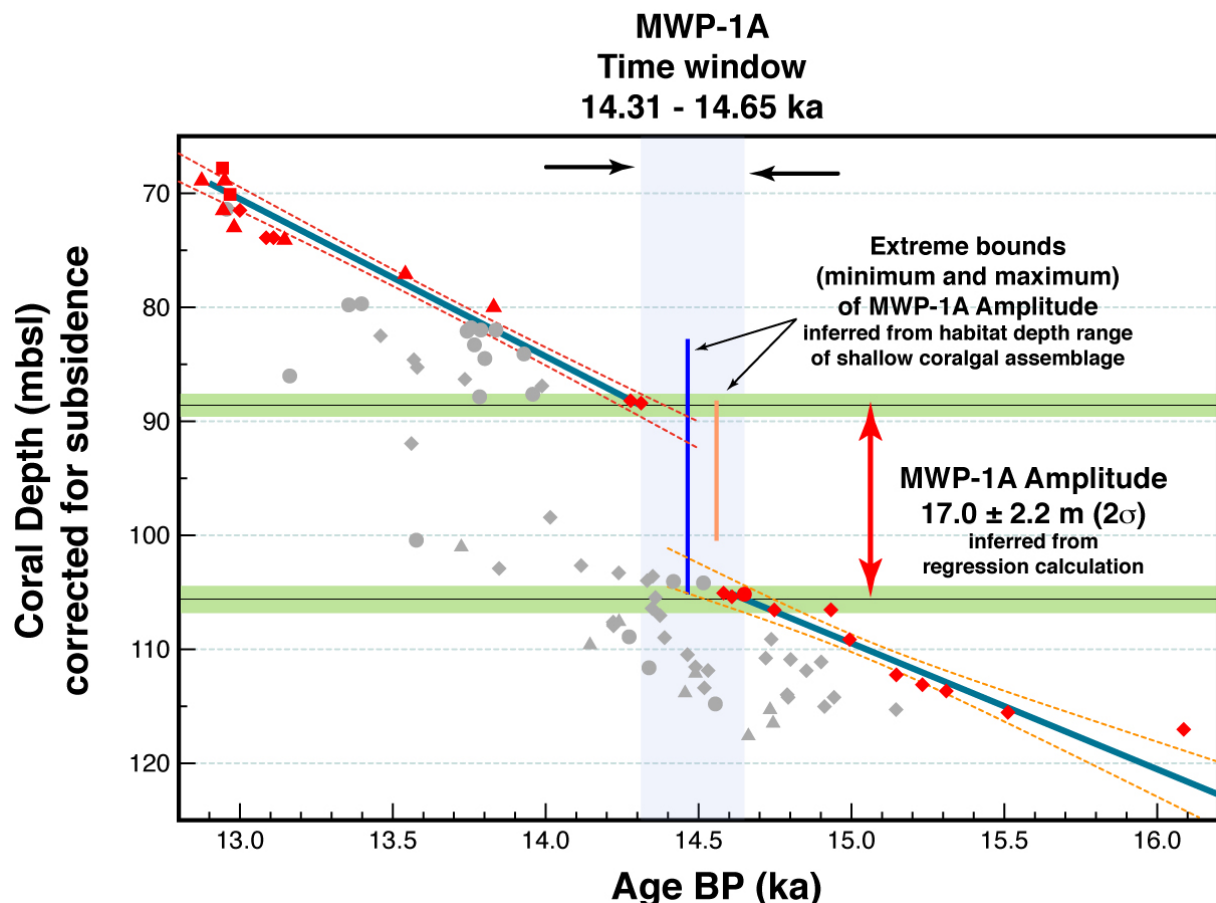
Figure S6: *MWP-1A amplitude estimate inferred from the gap between linear fits throughout the pre- and post-MWP-1A periods. Regression lines (in blue) and their 2σ error envelopes (in red and orange) were calculated using Isoplot 3.00 software[59]. Samples used for regression calculation are highlighted in red. Uncertainties in pre- and post-jump depths are shown*

by green horizontal bars and are calculated by considering the error envelopes at 14.65 ka and 14.31 ka. The two extreme bounds (i.e. 12 and 22 meters) of MWP-1A amplitude inferred from habitat depth range of shallow coralgal assemblage are also shown. This comparison shows that these two extreme are very unlikely, thus strengthening our preferred range (i.e. 14 to 18 meters) constrained by taking together the ecological requirements of multiple coralgal assemblages and the depositional context.

It could be questioned whether the difference in elevations between the stratigraphic units containing the dated corals should be considered to determine MWP-1A amplitude instead of the elevation of the relevant corals. The difference between the depth of the coral samples that we dated and the stratigraphic boundaries (limit of the biological "assemblages") is less than a meter (see Fig. S3) and therefore within the inherent uncertainty of the coral-based approach. This option will therefore also lead to an estimate of MWP-1A amplitude of ~16 meters.

Rate of sea-level rise during the jump

The detailed assessment of the timing and amplitude of MWP-1A sea-level change leads to an average rate of sea-level rise of 46 ± 6 mm/yr (i.e.16 ± 2 in 350 yr) at Tahiti during the event. Note that this value is only a minimum estimate, since we do not take into consideration any time lag in reef initiation on the submerged surface, nor the uncertainties related to the MWP-1A inception. Assuming an extreme scenario where MWP-1A started at 14.5 ka and terminated at 14.4 ka (see Fig. S4-b), the local rate of the sea-level rise associated to the MWP-1A event could have reached 160 ± 20 mm/yr.

Table S1: Age and estimated lower and upper bounds of the different tie points that define the Tahiti RSL curve. Points n°1 to 4 were previously defined by Bard et al.[24]. Numbers in parenthesis gives our preferred estimates.

	Age (ka)	IODP sample	Sea-Level estimate (mbsl)	
			Lower bound	Upper bound
Point n°1	9.000		29	27
Point n°2	11.600		58	56
Point n°3	12.850		67	65
Point n°4	12.900		69	67
Point n°5	14.312	310-M0023A- 13R-2W 32-37	88	83 (86)
Point n°6	14.650	310-M0015A- 37R-1W 19-28	105 (104)	100 (102)
Point n°7	14.933	310-M0011A- 6R-1W 24-35	107	105
Point n°8	15.310	310-M0025B- 11R-1W 70-74	114	109
Point n°9	16.087	310-M0009B- 15R-1W 13-20	117	109
Point n°10	19.000	arbitrary fixed at 119 mbsl	119	119

Tahiti RSL curve

By combining all these observations, we are also able to derive the lower and upper bounds of Tahiti RSL over the last deglaciation (see Table S1 and Figures 2, 3 and S4). For the 14 - 9 ka time window, we consider the tie points and sea-level rates previously determined by Bard et al.[24]. Note that the sea-level position at 19 ka was arbitrary fixed at 119 mbsl (see main text).

Reconciling the Tahiti and the Barbados record

The MWP-1A timeframe derived from the extended Tahiti record contradicts the previous timing inferred from the Barbados coral-reef record, which was also established on the basis of U-Th dating (see Fig. 3). In the latter, the MWP-1A was first identified between 14.2 and 13.8 ka, but a thorough re-examination of this record conducted Liu and Milliman[33] to reappraise this timing and to bracket the MWP-1A between 14.3 to 14.0 ka. Some studies have questioned this conventionally accepted Barbados timing[12,21], but most of the arguments raised against it have been contradicted by the updated data set provided by Fairbanks et al.[29] or Peltier and Fairbanks[19] that complemented the original record and refined previous ages through the use of improved analytical method. These new data suggest that the MWP-1A occurred even later than initially delineated by the original Barbados curve, i.e. between 14.08 and 13.61 ka. Whatever the data set considered for the Barbados record, it was generally argued that the MWP-1A coincided with the Older Dryas, the cooling event that terminated the Bølling warm period[14,16,33]. In contrast, the extended Tahiti record presented here indicates that the MWP-1A occurred at least 400 to 500 years earlier, and was therefore synchronous with the Bølling period (Fig. 2).

It is very unlikely that this discrepancy could be related to any analytical bias as the paired radiocarbon and U-Th analyses that were carried out on the Tahiti corals (voir Durand et al.[86] et Durand et al., ms in prep) as well as on Barbados corals[29] are highly consistent with the Intcal09 calibration curve for the relevant period[30]. The only way to reconcile the Barbados and Tahiti data sets is to consider that the onset of MWP-1A in the Barbados would correspond record to *A. palmata* samples RGF 15-5-3 and RGF 9-13-3 which were dated at about 14.550 ka BP[19]. In this respect, it can be noticed that the samples from Barbados hole 9, corresponding to the time interval spanning 14.55 to 14.08 ka BP, actually indicate an unusual and significant increase in the rate of sea level rise compared to the other part of the deglaciation (Fig. S7). Weaver et al.[12] also pointed out that the *A. palmata* sample RGF 9-8-2 dated at 14.08 ± 0.03 ka BP and generally considered as marking the start of the MWP-1A in the Barbados record is overlain by deeper-water species, *Porites asteroides* and *A. cervicornis*, suggesting that this sample may be part of a deepening-upward sequence which would have been already initiated earlier in response to the rapidly rising sea level. Another direct implication of this hypothesis is that *A. palmata* habitat is not limited to the 3 - 7m depth range[87] as it is generally assumed in the literature, but instead that this species may thrive in deeper reef environments[12], commonly deeper that 10 m and occasionally down to 20 m as supported by direct observations[88,89]. In addition, studies of the *A. palmata* distribution in modern reefs, may not be completely applicable to the deglaciation, a period during which sea level was rising at an average rate exceeding 10 mm/yr.
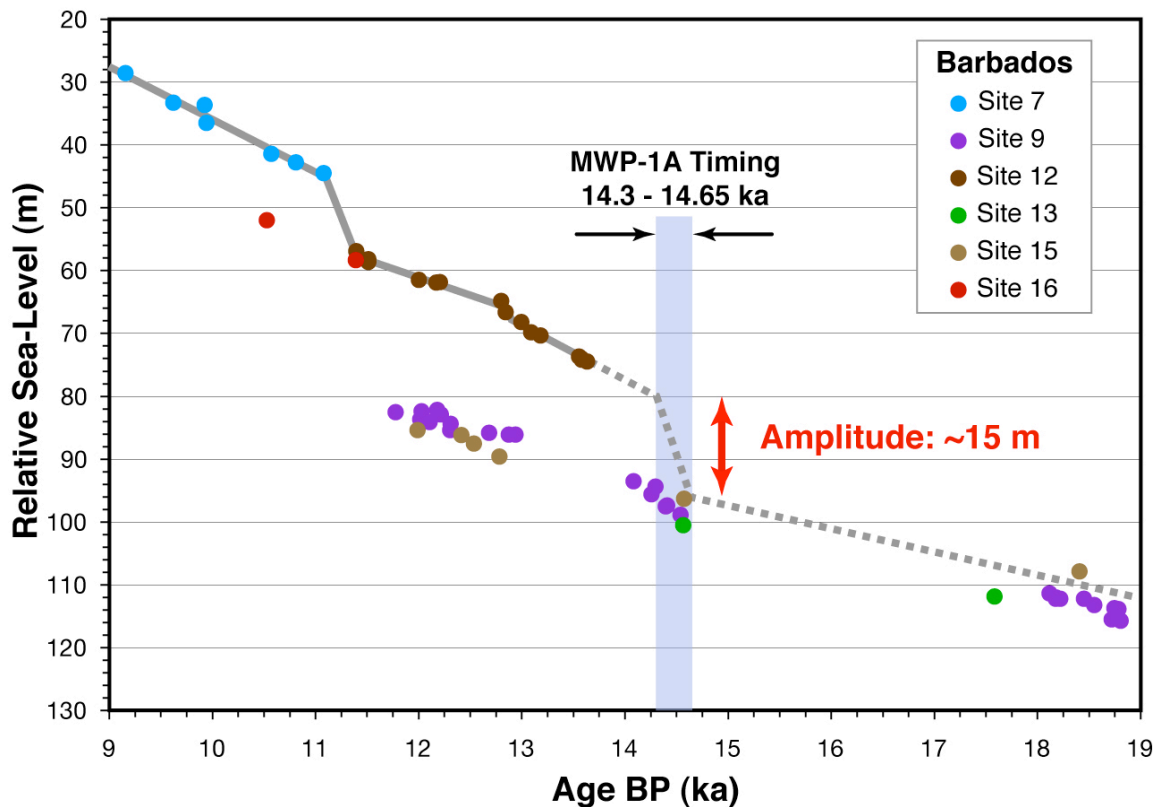
Figure S7: *Reappraisal of the amplitude of MWP-1A at Barbados considering the new MWP-1A chronozone inferred from the present study. Data from Fairbanks et al.[29] and Peltier and Fairbanks[19]. Over the 14.3 - 9 ka period, the dark grey line corresponds to the Barbados sea-level curve as determined by linear fits of sea-level data (here A. palmata). For the 13 - 9 ka time window, the calculations are done by considering specific time intervals related to known climatic boundaries (see Bard et al.[24] for more details).*

This re-evaluation of the MWP 1A timeframe also requires a reassessment of the MWP-1A amplitude at Barbados. Assuming a 350 yr duration of MWP-1A, and extrapolating the general trend line delineated by hole 12 for the period following the jump (see Fig. S7), we can derive a ~15 m amplitude of sea-level rise at Barbados during the MWP-1A time window.

Reappraisal of the Sunda Shelf record
The Sunda Shelf record obtained by Hanebuth et al.[8] on mangrove organic material of a shallow siliciclastic platform describes a very sharp sea-level jump between 14.6 and 14.3 ka (see Fig. 3 and Fig. S8). Scepticism has first been expressed on the timeframe of this record as it relies on AMS ^{14}C ages, which are subject to much greater uncertainty than U-Th chronologies and may be significantly hampered by the occurrence of radiocarbon plateaus that prevent any high-resolution chronology[16]. This is particularly problematic in the present case because the ^{14}C ages of samples that marked the MWP-1A event in the Sunda record coincide with the 500-year-long ^{14}C plateau overlapping with the Bølling period[30]. The samples that marked MWP-1A

event closely cluster around a conventional ^{14}C age of 12.415 ± 0.032 ka BP (1 SD, n = 17).
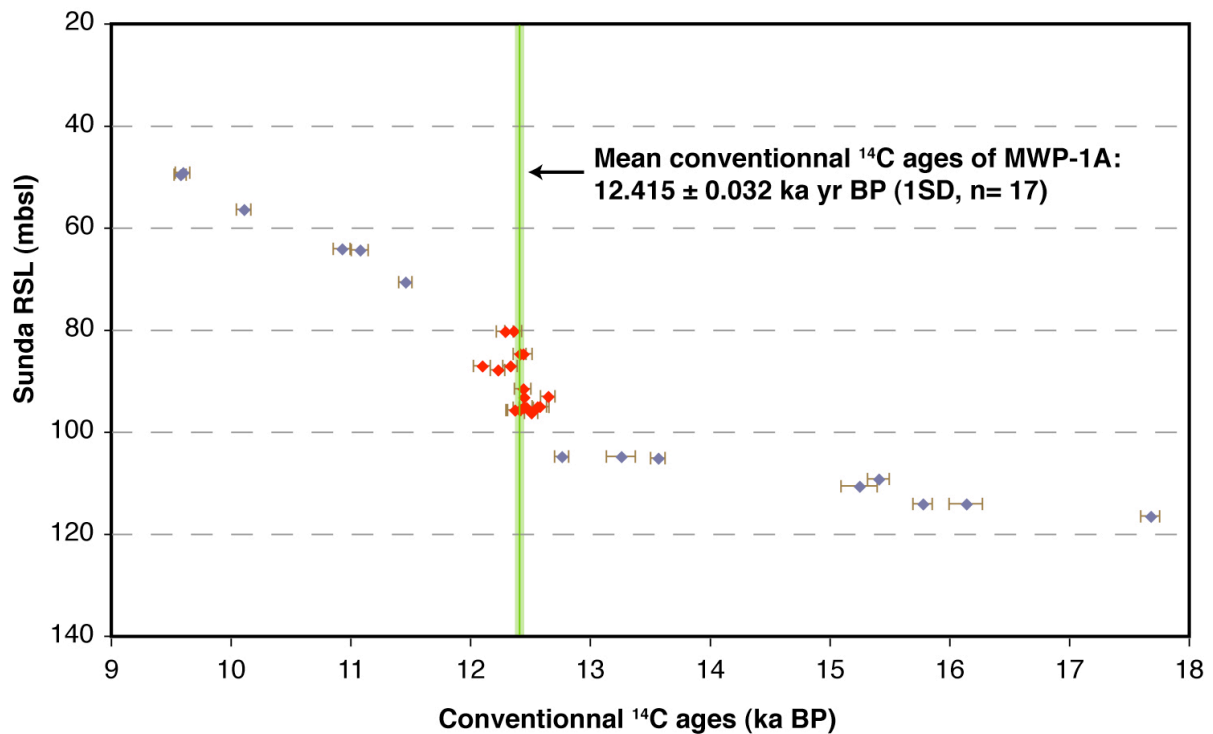
Figure S8: *Sea-level record from the Sunda Shelf. Data from Hanebuth et al.[8]. [14]C ages are conventional (uncalibrated) ages in yr BP with statistical errors given at 1 σ, which does not include the error in the reservoir age correction.*

This mean age for the MWP-1A event is derived by averaging ^{14}C ages of all samples contained between 80 and 100 mbsl in the Sunda shelf record. In doing this, we hypothesize that the MWP-1A is a sufficiently abrupt and sharp event to be considered as the brief spell marked by the samples contained within this depth interval. Bearing in mind the scatter and uncertainty in the ^{14}C dataset (see Fig. S5), this approach seems suitable. This conventional ^{14}C timeframe makes MWP-1A coeval with the onset of the Bølling that have been dated at 12.46 ± 0.15 ^{14}C ka BP in North Atlantic sediments[90]. Using the IntCal09 calibration curve[30], the mean calendar age of the "Sunda" MWP-1A can be refined to the 1σ interval 14.18 - 14.62 ka BP, or to 14.14 - 14.94 ka BP considering the 2σ interval. Although these uncertainties remain large, this age interval is consistent with the MWP-1A chronozone inferred from the new Tahiti record, but does not display any overlap with that previously based on the Barbados record[19,29].

Numerical modelling of reef growth in response to a MWP

We used a 2D numerical model previously constructed and used by Bard et al.[14,91] to simulate the building of the Tahiti coral reef in response to MWP-1A. It includes the simultaneous effects of sea-level fluctuations, local subsidence/uplift and reef growth on the development and the internal structure of a reef system. The model is based

on equations described in Bosscher and Schlager[92], which combines the skeletal growth of reef-building corals (where photosynthetic rate, calcification rate, and skeletal growth rate are proportional) and the Beer-Lambert's law that describes the light distribution in the water column. Thus, the coral reef vertical growth rate is a function of water depth. Moreover, the model offers the possibility to display age-depth relationships along virtual drill holes at different locations in the reef structure. This approach is especially useful to compare the model outputs with data derived from real holes or to identify key sites for future drilling operation. For the present study, the model has been updated and now takes into account continental and marine erosion modelled using a diffusion law[93,94]. This update will be presented in more details elsewhere. Note that similar models have been used to simulate reef growth over longer time scales[95,96], but not with the specific purpose to investigate the reef response to MWPs.

Here, we operate this model over the last deglaciation by considering a simplified sea-level curve derived from the Tahiti onshore and offshore records (see the curve in Fig. 2). The input sea-level curve is shown on Fig. S9-a&b and Fig. S10-a (thick blue curve). The rates of the sea-level rise for the different time windows of the curve are as follows: 19 - 16.09 ka, 0.7 mm/yr; 16.09 - 14.93 ka, 9.1 mm/yr; 14.93 - 14.65 ka, 8.9 mm/yr; 14.65 - 14.31 ka, 45.9 mm/yr; 14.31 - 14 ka, 20.3 mm/yr; 14 - 12.9 ka, 12.1 mm/yr; 12.9 - 11.6 ka, 8.6 mm/yr; 11.6 - 9 ka, 11.2 mm/yr; 9 - 5 ka, 7.2 mm/yr; 5 to the present, 0 mm/yr. The amplitude of the sea-level jump corresponding to MWP-1A is thus 15.6 m during 340 years. For the sake of clarity, the part of the reef which accreted during the MWP-1A event is coloured in red (see Fig. S9-c and S10-b). The coloured curves within the cross-section represent isochron topographies drawn every 500 years (see the colour bar at the right of Fig. S9-c and Fig. S10-c). The x-axis is the distance seaward, and the y-axis is the depth.

In the present study, the model was run considering two different initial topographies for the Pleistocene substrate. Fig. S9 displays the outputs of the model with a constant slope for the Pleistocene basement. For this simulation, the following parameters have been used: subsidence rate = 0.25 mm/yr, growth rate = 13 mm/yr; radiation extension coefficient k = 0.125; light saturation: the fraction of the surface light irradiation needed for maximum reef growth ($I_0 I_k^{-1}$) = 6 (light saturation at about 15% of the surface value); erosion diffusion coefficient Kd = 0.01 m^2/yr.

The age-depth relations simulated in different vertical and deviated holes drilled onshore (drill n°1 to n°3) on the present-day reef and offshore (drill n°4, see Fig. S9-c) are shown in Fig. S9-b&c. These simulations clearly illustrate that onshore drill holes are only capable of recovering reef material after MWP-1A. Post MWP-1A reef shows a general keep-up development and substantiates previous results obtained by Bard et al.[14,24] on P6 to P10 onshore holes. Moreover, these simulations highlight the fact that the deviated hole (drill n°3) records older and deeper corals than the vertical hole (drill n°2) (see Fig. S9-a). This is in agreement with the results obtained on onshore drill holes, where corals of the lower section of the deviated P8 hole plot slightly lower than those of the vertical P7 hole[24]. Conversely, offshore drill holes (drill n°4) enabled recovery of corals accreted before MWP-1A, but record a deepening sequence after the MWP-1A event (Fig. S9-b), in agreement with new data presented in this study (e.g. Sites M0024 and M0009; see Fig. 2 and Fig. S2).
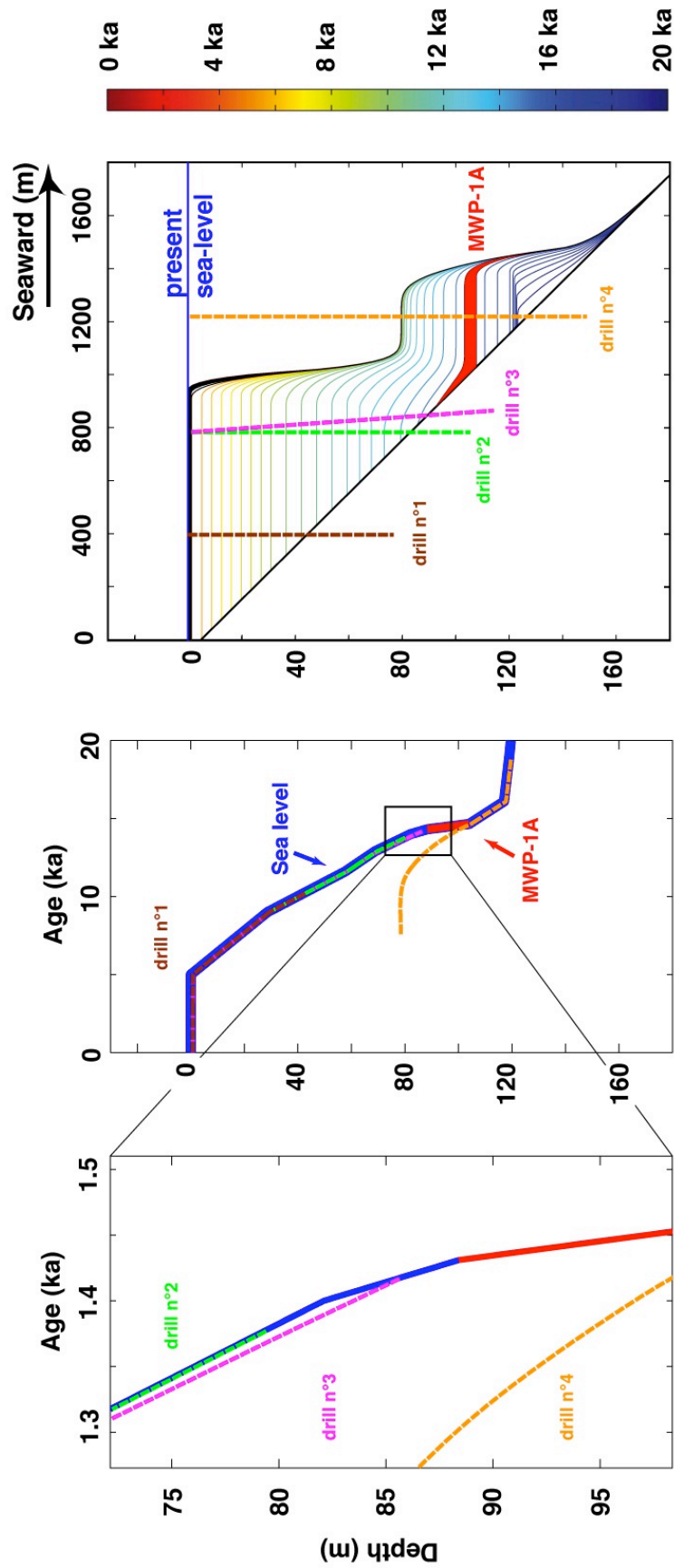
Figure S9. Two-dimensional structure of a modelled reef developed on constant slope during the last 20 ka in response to MWP-1A.
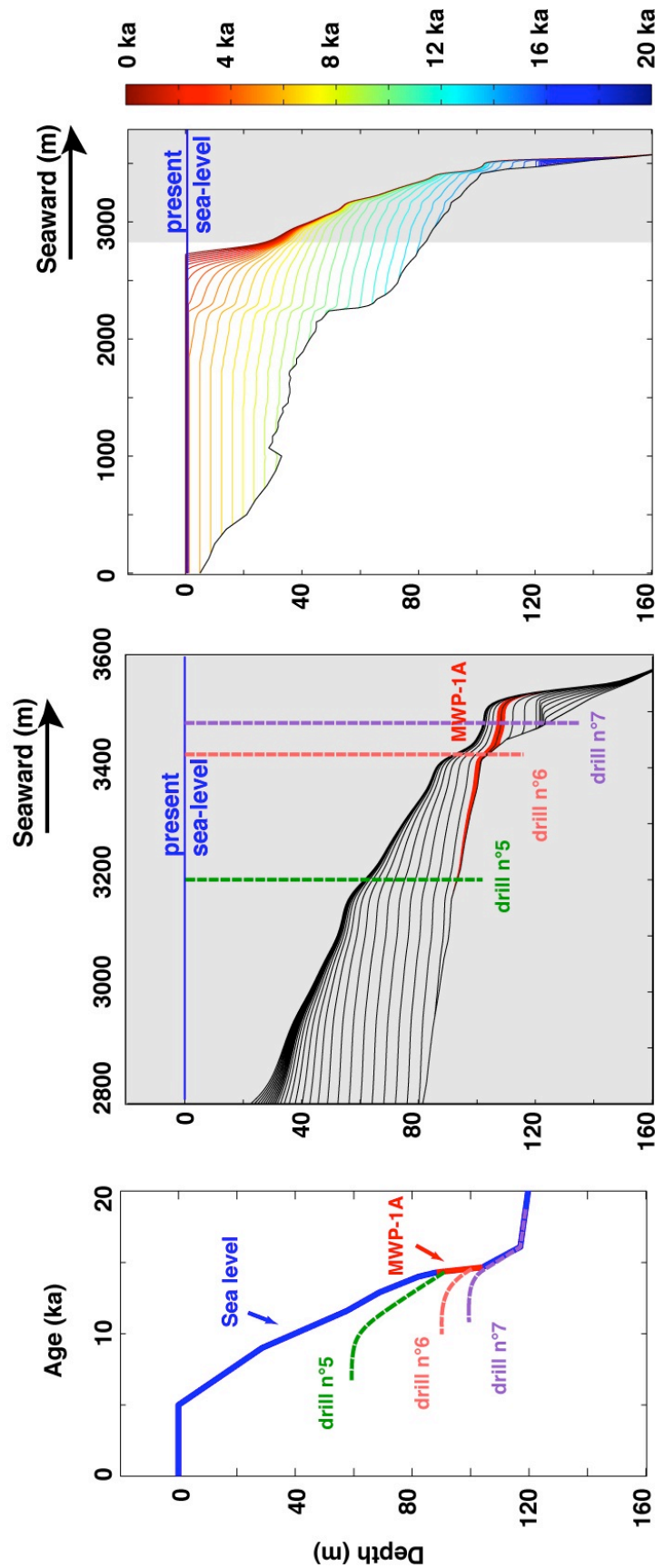
Figure S10: Two-dimensional structure of a modelled reef developed during the last 20 ka in response to a rapid MWP (same timing and amplitude than in

Fig. S2). The basement substrate (corresponding to the Pleistocene / post-glacial boundary) used in this figure is obtained from the seismic and multibeam bathymetric data produced during the SISMITA cruise[97].

Our model was also run considering the real topography of the basement substrate (corresponding to the Pleistocene / post-glacial boundary) as inferred from seismic and multibeam bathymetric data produced during the SISMITA cruise[97]. Fig. S10-c displays the overall internal reef structure, along a seaward transect, accreted during the last 20 ka while Fig. S10-b is a blow-up of the model output in the outer part of the reef system (location indicated by the grey area in Fig. S10-c). The sea level curve and the parameters used for this model (Fig. S10-b) are the same than those in Fig. S9 (see Fig. S9-b), except for the growth rate which is 8 mm/yr. As shown in Fig. S10-b, the stratigraphic level corresponding to MWP-1A is very thin. In Fig. S10-a, the age-depth record, simulated by the model, is displayed for 3 virtual vertical holes whose locations are indicated in Fig. S10-c.

For virtual holes drilled in the outer edge of the system (drill n°7), the reef growth model simulates a general upward growth before MWP-1A, followed by a deepening-upward trend after the MWP-1A spell. A further point worth emphasizing is that, as depicted by drill n°6 record, the reef system failed to keep pace with sea-level rise during the entire MWP-1A interval. This is highly consistent with observational data obtained during the course of this study (Site M0005, see Fig. 2 and Fig. S2). Only holes collected in intermediate position on the fore-reef slope (drill n°5) between the outer edge and the modern reef are able to capture the sea-level position immediately following MWP-1A. It is also noteworthy that our present model does not take into account any time lag in reef initiation. However, after MWP-1A, the reef experienced a deepening event which was weaker than that observed on the outer edge of the reef system. This phenomenon is observed in the key IODP Site M0023.

GIA model

Model predictions of the glacio-hydro-isostatic adjustment (GIA) were conducted using the parameters described elsewhere[98-101]. The model included both an earth component describing the viscoelastic nature of the solid earth and an ice component documenting the history of ice melting reconstructed mainly from far-field sea-level observations[9,102,103]. This model provides an accurate treatment of time-dependent continental shorelines[101], but does not take into consideration the feedback onto sea level from Earth-rotation changes. We employed the same earth model parameters as used by Bassett et al.[20] with a lithosphere thickness of 100 km and sublithospheric upper mantle viscosity of 5.10^{20} Pa.s. For the lower mantle viscosity, we consider the high-viscosity lower mantle value (4.10^{22} Pa.s) adopted by Bassett et al.[20]. We also generate a suite of GIA predictions by varying the viscosity of the lower mantle from 10^{22} Pa.s to 10^{23} Pa.s in order to assess the sensitivity of GIA results to variations in the visco-elastic Earth model.

This ice model was tuned in such a way that the eustatic sea level (ESL) rise during MWP-1A chronozone represents 14 meters of eustatic amplitude (ESL curve shown in Fig. S11-e&b). The term eustatic refers here to the sea-level change

associated with the change in ocean volume resulting from the melting or growth of land-based ice sheets (i.e., the total meltwater volume divided by the area of the ocean, taking into consideration its variation through time). This definition corresponds to the one used by Clark et al.[36] and Milne and Mitrovica[27] and is equivalent to the "ice-volume equivalent sea-level change" defined by Lambeck et al.[104].

RSL predictions at Tahiti and Barbados derived from this GIA model are illustrated in Fig. S11. We have considered three distinct melting scenarios in which the respective contributions of the Antarctic Ice sheet and the Northern Hemisphere Ice Sheet vary from 20:80 (Fig. S11-e&f), 50:50 (Fig. S11-c&d) to 80:20 (Fig. S11-a&b). The ice model was slightly adjusted to account for the newly obtained timing and magnitude of MWP-1A from Tahitian sea level observations. This ice model allows us to determine the Eustatic Sea-Level (ESL) curve depicted in Fig. S11-e. Note that it is this ESL curve that we use to calculate the ESL rate depicted in Fig. 3.

Only the 80:20 scenario provides a satisfactory fit to the Tahiti record. Both the 20:80 scenario (Fig. S11-e), and the 50:50 scenario (Fig. S11-c), under-evaluate the post-MWP-1A sea level at Tahiti, by more than 10 m. This general tendency is in agreement with previous studies that demonstrated that increasing the Antarctic contribution to MWP-1A reduces the magnitude of the sea-level jump at the Tahiti far-field site relative to that at Barbados[20,36,105].

In contrast, our GIA predictions tend to predict sea level a few meters deeper than deduced at Barbados over the entire deglaciation period, when the optimal value of the viscosity (4.10^{22} Pa.s) adopted by Bassett et al. [20] is considered. In this case, only the 20:80 scenario provides an acceptable fit to the Barbados data. However, increasing the value for the lower mantle viscosity to 10^{23} Pa.s reduces this discrepancy, whatever the South:North melting scenario.

The large discrepancy between observed and predicted post-MWP-1A sea level at Tahiti for the 20:80 scenario allows us to rule out a melting scenario involving a dominant North Hemisphere source for MWP-1A. Owing to the uncertainties in the Earth model parameters and second order misfits observed between predictions and observational constraints from Tahiti and Barbados, it remains difficult at this stage to go further in the quantification of the respective contributions of North and South Hemisphere to MWP-1A. However, these results, together with previous studies[20,36] substantiate the hypothesis of a substantial AIS contribution to MWP-1A, that very likely represented half, or more, of equivalent eustatic sea-level rise observed during this event.

Our GIA experiments have been conducted considering an ice model that imposes a eustatic rise of 14 m during the MWP-1A time window. No experiment has been carried out to assess the sensitivity of the GIA outputs to this value. However, the relationship between ESL and RSL is consistent with the Clark et al.' study[36] that provides a comparison of sea-level fingerprintings arising from MWP-1A at different far-field sites. These authors show that the RSL amplitude of MWP-1A recorded at Tahiti should be amplified with respect to the ESL amplitude whatever its source(s). Indeed, they calculated that the MWP-1A amplitude observed at Tahiti is amplified by about ~10%, ~20% and ~30% if MWP-1A is sourced from WAIS, the entire AIS or LIS, respectively.

Considering our preferred 14 - 18 m range of RSL amplitude for MWP-1A at Tahiti, we can derive a 10 - 16 m range for the ESL jump related to the MWP-1A

event. Note that this range is estimated by considering all possible MWP-1A source(s) and that it is considerably less than previous estimates.
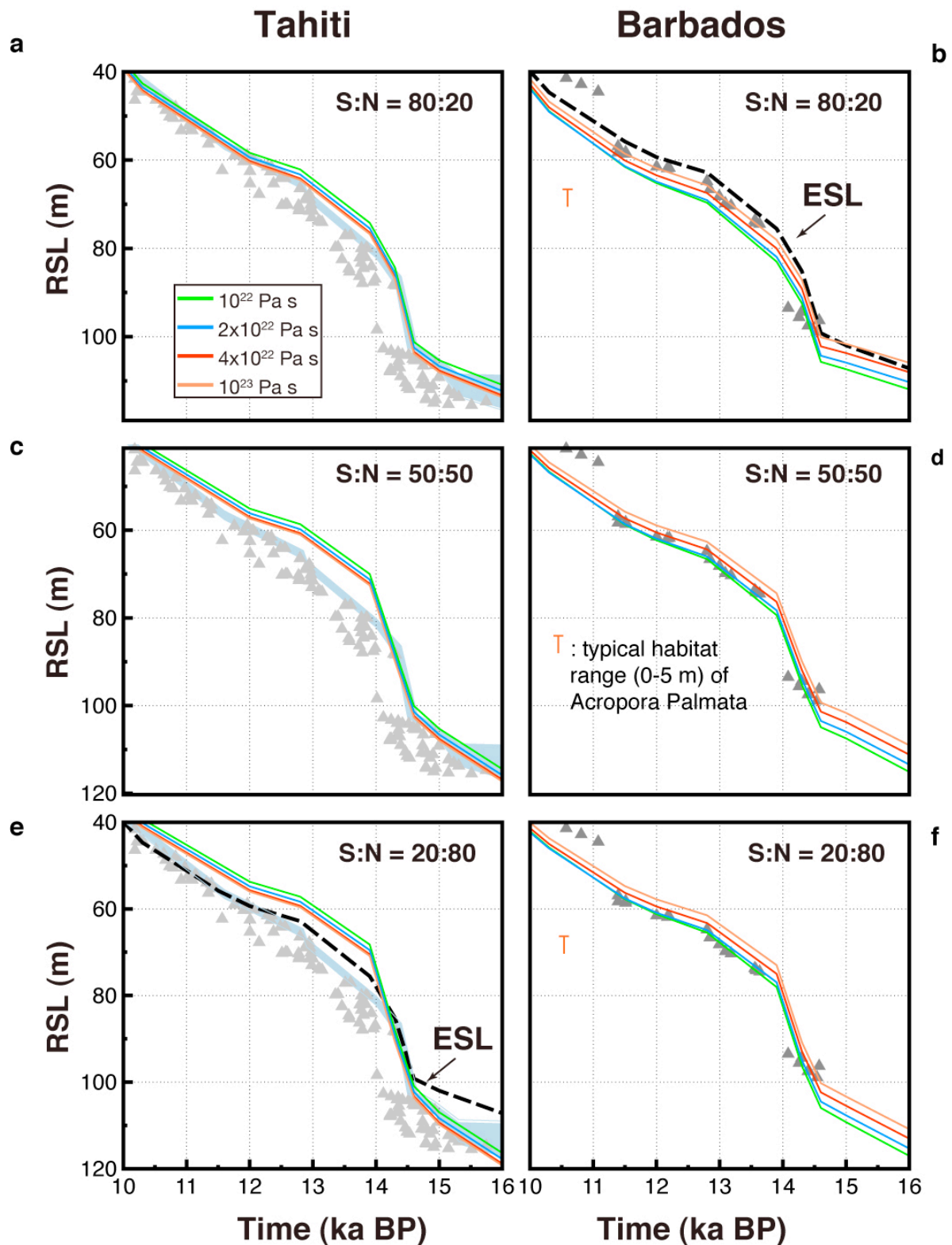
Figure S11: *Numerical RSL predictions at Tahiti and Barbados for varying AIS and NHIS contributions to the MWP-1A event and for distinct values of the*

lower mantle viscosity. The blue bands for the Tahiti plots correspond to our preferred estimate of Tahiti RSL (see Fig. S4a).

Table S2: U-Th ages and coral description

Activity ratios and ages are calculated using the new decay constants determined by Cheng et al.[58]. All reported errors are given at the 2σ level. Labels #1, #2, etc, stands for replicated analyses obtained on different pieces of the same coral sample. U-Th ages are calculated using the Isoplot software[59]. No correction for detrital ^{230}Th were processed because ^{232}Th concentrations are in most cases low (≤ 0.5 ppb). Ages are presented in years before 1950 AD. Coral types are: mp, massive *Porites* sp.; bp, branching *Porites* sp; ep, encrusting *Porites* sp; rbp, robust branching *Pocillopora* sp.; bpo, branching *Pocillopora* sp; ta, tabular *Acropora* sp.; ra, robust *Acropora*; ep, encrusting *Porites* sp.; ba, branching *Acropora* sp.; em, encrusting *Montipora* sp.; mm, massive *Montipora* sp; fm, foliacious *Montipora* sp; pa, *Pavona* sp; ml, massive *Leptastrea* sp. Coralgal assemblages are: PM, robust branching *Pocillopora*/massive *Montipora* (0 - 10 m); mP: massive *Porites* (0 - 20 m); tA: tabular *Acropora* (5 - 15 m); PP: branching *Porites*/*Pocillopora* (5 - 15 m); PPM: branching *Porites*/encrusting *Porites* and *Montipora* (5-25 m); AFM: encrusting *Agaricid* and *Faviid* (> 20 m). Occurrence of vermetid gastropod that is indicative of very shallow environment (> 5 m) is indicated by asterisk.

Location	IODP Sample ID	Coral Species	In situ / Reworked	Coralgal Assemblages	Depth (mbsl)	Corrected Depth	Analytical technique		^{238}U ppb	^{232}Th ppb	$(^{230}$Th/^{238}U$)$	$(^{234}$U/^{238}U$)$	$(^{238}$U/^{232}Th$)$	Age ka (BP)	$(^{234}$U/^{238}U$)_0$
Maraa															
	310-M0005A- 12R-1W 51-54	mp	IS	mP	75.2	72.5	TIMS		2402.6 ± 3.1	0.154 ± 0.000	0.1105 ± 0.0001	1.1423 ± 0.0005	47777 ± 96	11.03 ± 0.02	1.1468 ± 0.0005
	310-M0005C- 11R-1W 46-59	ta	IS	tA	80.0	77.0	TIMS	#1	3468.9 ± 4.4	0.043 ± 0.000	0.1181 ± 0.0002	1.1419 ± 0.0005	245297 ± 588	11.84 ± 0.02	1.1467 ± 0.0005
							TIMS	#2	3434.4 ± 4.4	0.085 ± 0.001	0.1183 ± 0.0003	1.1421 ± 0.0006	123852 ± 750	11.86 ± 0.03	1.1470 ± 0.0006
							TIMS	#3	3458.1 ± 4.4	2.173 ± 0.016	0.1178 ± 0.0003	1.1419 ± 0.0006	4863 ± 37	11.80 ± 0.04	1.1468 ± 0.0006
							TIMS	#4	3461.5 ± 4.6	0.081 ± 0.000	0.1174 ± 0.0001	1.1422 ± 0.0008	131277 ± 270	11.75 ± 0.02	1.1470 ± 0.0008
							MC-ICPMS	#5	3343.5 ± 0.9	0.081 ± 0.001	0.1181 ± 0.0002	1.1404 ± 0.0010	125346 ± 1991	11.86 ± 0.02	1.1452 ± 0.0010
							MC-ICPMS	#6	3406.7 ± 0.5	0.046 ± 0.001	0.1186 ± 0.0002	1.1402 ± 0.0010	225055 ± 3575	11.91 ± 0.02	1.1450 ± 0.0010
	310-M0005D- 2R-1W 107-115	bpo	IS	PM*	85.1	82.0	TIMS		2623.4 ± 3.3	0.794 ± 0.001	0.1236 ± 0.0002	1.1419 ± 0.0005	10104 ± 21	12.43 ± 0.03	1.1470 ± 0.0005
	310-M0005D- 5R-2W 0-5	bp	Rew		89.3	86.0	TIMS		2736.4 ± 3.6	0.184 ± 0.000	0.1305 ± 0.0004	1.1416 ± 0.0009	45382 ± 112	13.16 ± 0.04	1.1470 ± 0.0010
	310-M0005D- 6R-1W 23-31	rbp	IS	PM*	91.1	87.6	MC-ICPMS		2839.9 ± 3.5	1.618 ± 0.029	0.1375 ± 0.0005	1.1392 ± 0.0008	5360 ± 95	13.96 ± 0.05	1.1448 ± 0.0009
	310-M0005D- 6R-2W 0-5	mm	IS	PM*	91.3	87.9	TIMS	#1	3558.2 ± 4.6	0.623 ± 0.001	0.1357 ± 0.0003	1.1403 ± 0.0008	17445 ± 39	13.74 ± 0.04	1.1459 ± 0.0008
							MC-ICPMS	#2	3672.6 ± 4.6	0.610 ± 0.011	0.1368 ± 0.0005	1.1399 ± 0.0008	18388 ± 325	13.87 ± 0.05	1.1456 ± 0.0009
	310-M0007A- 18R-1W 77-109	mp	IS	mP	61.6	59.1	TIMS		2750.6 ± 3.5	0.565 ± 0.001	0.1011 ± 0.0002	1.1433 ± 0.0006	14877 ± 31	10.03 ± 0.02	1.1474 ± 0.0006
	310-M0007B- 21R-1W 0-20	mp	IS	mP	67.1	64.3	MC-ICPMS		2481.4 ± 0.4	0.467 ± 0.003	0.1107 ± 0.0004	1.1417 ± 0.0009	16223 ± 107	11.06 ± 0.04	1.1462 ± 0.0009
	310-M0015A- 33R-1W 29-40	bpo	IS	PP	103.8	100.4	TIMS	#1	2834.9 ± 3.7	0.209 ± 0.000	0.1346 ± 0.0004	1.1404 ± 0.0006	41534 ± 111	13.62 ± 0.04	1.1459 ± 0.0007
							TIMS	#2	2831.9 ± 3.6	0.232 ± 0.000	0.1340 ± 0.0002	1.1405 ± 0.0007	37355 ± 84	13.56 ± 0.03	1.1460 ± 0.0007
	310-M0015A- 36R-1W 51-52	mm	IS	PM	107.7	104.1	TIMS		3640.8 ± 4.7	1.084 ± 0.002	0.1419 ± 0.0002	1.1397 ± 0.0005	10262 ± 21	14.42 ± 0.03	1.1455 ± 0.0005
	310-M0015A- 36R-2W 0-6	mm	IS	PM	107.8	104.2	TIMS		3738.7 ± 4.8	0.802 ± 0.001	0.1427 ± 0.0002	1.1393 ± 0.0006	14252 ± 29	14.52 ± 0.03	1.1452 ± 0.0006
	310-M0015A- 37R-1W 19-28	mm	IS	PM	108.8	105.2	TIMS		3501.6 ± 4.5	0.284 ± 0.000	0.1439 ± 0.0002	1.1392 ± 0.0007	37719 ± 79	14.65 ± 0.02	1.1451 ± 0.0007
	310-M0016A- 36R-2W 5-10	mp	IS	mP	118.4	114.8	TIMS		2553.1 ± 3.2	0.161 ± 0.000	0.1431 ± 0.0002	1.1396 ± 0.0005	48324 ± 98	14.56 ± 0.02	1.1455 ± 0.0006
	310-M0018A- 7R-1W 73-82	ta	IS	tA	92.1	89.2	TIMS		3320.8 ± 4.2	0.651 ± 0.001	0.1149 ± 0.0003	1.1429 ± 0.0005	15582 ± 32	11.49 ± 0.03	1.1477 ± 0.0005
	310-M0018A- 18R-1W 40-50	mp	IS	mP	112.5	108.9	TIMS		2405.6 ± 3.1	0.135 ± 0.000	0.1407 ± 0.0006	1.1407 ± 0.0007	54595 ± 162	14.27 ± 0.06	1.1465 ± 0.0007
	310-M0018A- 19R-1W 107-110	mp	IS	mP	115.2	111.6	TIMS		2684.6 ± 3.6	0.846 ± 0.001	0.1411 ± 0.0002	1.1393 ± 0.0006	9694 ± 21	14.34 ± 0.03	1.1451 ± 0.0006
Tiaeri															
	310-M0009A- 6R-1W 38-48	mp	IS	PPM	106.9	103.3	MC-ICPMS		2758.2 ± 0.5	1.832 ± 0.002	0.1401 ± 0.0003	1.1390 ± 0.0009	4598 ± 5	14.24 ± 0.03	1.1447 ± 0.0009
	310-M0009A- 9R-1W 19-22	pa, em	IS	PPM	110.6	107.0	MC-ICPMS		3588.9 ± 0.5	3.196 ± 0.003	0.1413 ± 0.0003	1.1382 ± 0.0009	3430 ± 3	14.37 ± 0.03	1.1439 ± 0.0009
	310-M0009B- 9R-2W 0-5	rbp	Rew?	PPM	110.0	106.4	TIMS	#1	2879.7 ± 3.7	0.184 ± 0.000	0.1411 ± 0.0003	1.1400 ± 0.0005	47732 ± 121	14.33 ± 0.03	1.1458 ± 0.0005
							TIMS	#2	3006.5 ± 3.9	0.709 ± 0.001	0.1414 ± 0.0003	1.1395 ± 0.0006	12965 ± 29	14.37 ± 0.03	1.1453 ± 0.0007
	310-M0009B- 13R-1W 11-18	ta	IS	tA	117.0	113.4	TIMS		3291.2 ± 4.2	1.701 ± 0.002	0.1427 ± 0.0002	1.1393 ± 0.0005	5912 ± 11	14.52 ± 0.02	1.1451 ± 0.0005
	310-M0009B- 14R-1W 22-25	rbp	IS	PM	119.1	115.3	TIMS		3138.3 ± 4.1	2.472 ± 0.004	0.1481 ± 0.0002	1.1368 ± 0.0010	3881 ± 8	15.15 ± 0.02	1.1428 ± 0.0011
	310-M0009B- 15R-1W 13-20	rbp	IS	PM	121.0	117.0	TIMS	#1	2937.2 ± 3.8	0.369 ± 0.002	0.1564 ± 0.0006	1.1395 ± 0.0009	24332 ± 108	16.02 ± 0.07	1.1460 ± 0.0009
							MC-ICPMS	#2	2941.2 ± 0.3	0.134 ± 0.001	0.1570 ± 0.0005	1.1369 ± 0.0008	66833 ± 412	16.13 ± 0.05	1.1433 ± 0.0009
	310-M0009C- 6R-1W 38-43	em	IS	AFM	106.4	102.9	TIMS		2815.5 ± 3.7	0.848 ± 0.001	0.1368 ± 0.0003	1.1409 ± 0.0007	10142 ± 22	13.85 ± 0.03	1.1466 ± 0.0007
	310-M0009C- 11R-2W 0-4	mp	IS	mP	111.5	107.9	MC-ICPMS		3090.4 ± 4.7	1.340 ± 0.005	0.1396 ± 0.0004	1.1366 ± 0.0005	7042 ± 28	14.22 ± 0.04	1.1422 ± 0.0006
	310-M0009C- 13R-2W 15-18	mp	IS	mP	114.1	110.5	MC-ICPMS		2802.1 ± 0.4	0.514 ± 0.002	0.1418 ± 0.0003	1.1365 ± 0.0005	16645 ± 61	14.46 ± 0.03	1.1422 ± 0.0006
	310-M0009C- 16R-1W 3-4	em	IS ?	mP	118.0	114.2	MC-ICPMS		4016.2 ± 0.6	0.556 ± 0.002	0.1464 ± 0.0003	1.1379 ± 0.0005	22060 ± 81	14.94 ± 0.03	1.1438 ± 0.0006
	310-M0009C- 17R-2W 0-10	mp	IS	mP	119.4	115.5	TIMS		2616.3 ± 3.4	0.798 ± 0.001	0.1518 ± 0.0002	1.1391 ± 0.0008	10014 ± 20	15.51 ± 0.03	1.1453 ± 0.0008
	310-M0009D- 7R-1W 11-28	mp	IS	mP	111.2	107.6	TIMS		2594.0 ± 3.3	0.262 ± 0.001	0.1401 ± 0.0005	1.1401 ± 0.0007	30230 ± 106	14.22 ± 0.06	1.1459 ± 0.0007
	310-M0009D- 7R-1W 28-45	mp	IS	mP	111.3	107.8	TIMS	#1	2603.8 ± 3.3	0.213 ± 0.000	0.1400 ± 0.0002	1.1403 ± 0.0005	37390 ± 74	14.20 ± 0.02	1.1460 ± 0.0005
							MC-ICPMS	#2	2470.9 ± 0.5	0.405 ± 0.001	0.1402 ± 0.0003	1.1384 ± 0.0005	18625 ± 69	14.26 ± 0.03	1.1442 ± 0.0006
	310-M0009D- 7R-2W 64-71	rbp	IS	PP	112.6	109.0	MC-ICPMS		2579.4 ± 0.4	0.436 ± 0.002	0.1414 ± 0.0003	1.1385 ± 0.0005	18054 ± 66	14.39 ± 0.03	1.1443 ± 0.0006
	310-M0009D- 9R-1W 66-77	bp	IS	PP	115.2	111.5	TIMS		3046.9 ± 3.9	1.647 ± 0.003	0.1425 ± 0.0003	1.1393 ± 0.0005	5652 ± 12	14.49 ± 0.03	1.1452 ± 0.0005
	310-M0009D- 9R-1W 99-103	mp	IS	mP	115.5	111.9	TIMS		3045.6 ± 3.9	0.947 ± 0.002	0.1429 ± 0.0004	1.1394 ± 0.0004	9828 ± 22	14.53 ± 0.05	1.1452 ± 0.0004
	310-M0009D- 10R-2W 74-78	mp	IS	mP	117.7	114.0	MC-ICPMS		2889.8 ± 0.4	1.145 ± 0.004	0.1450 ± 0.0003	1.1377 ± 0.0005	7707 ± 28	14.79 ± 0.03	1.1436 ± 0.0006
	310-M0009D- 10R-2W 96-107	mp	IS	mP	117.9	114.2	TIMS	#1	2523.7 ± 3.2	0.615 ± 0.001	0.1448 ± 0.0004	1.1396 ± 0.0009	12549 ± 28	14.75 ± 0.04	1.1456 ± 0.0009
							MC-ICPMS	#2	2643.5 ± 0.4	0.943 ± 0.003	0.1451 ± 0.0003	1.1366 ± 0.0005	8558 ± 32	14.82 ± 0.03	1.1425 ± 0.0006
	310-M0009D- 11R-1W 13-26	mp	IS	mP	118.8	115.0	TIMS	#1	2601.1 ± 3.4	2.929 ± 0.005	0.1466 ± 0.0004	1.1395 ± 0.0008	2714 ± 5	14.94 ± 0.04	1.1456 ± 0.0008
							MC-ICPMS	#2	2697.9 ± 0.4	6.744 ± 0.025	0.1458 ± 0.0003	1.1366 ± 0.0005	1222 ± 4	14.90 ± 0.03	1.1425 ± 0.0006
	310-M0009E- 7R-1W 5-17	mp	IS	mP	106.2	102.7	TIMS		2539.1 ± 3.2	0.439 ± 0.001	0.1391 ± 0.0004	1.1399 ± 0.0005	17675 ± 38	14.12 ± 0.04	1.1456 ± 0.0005
	310-M0009E- 9R-1W 32-36	em	IS	PP	109.1	105.5	MC-ICPMS		2456.3 ± 0.3	0.428 ± 0.001	0.1413 ± 0.0003	1.1395 ± 0.0009	17516 ± 25	14.36 ± 0.04	1.1453 ± 0.0009
	310-M0009E- 9R-1W 69-73	rbp	Rew	PP	109.4	105.7	MC-ICPMS		2798.8 ± 0.4	0.627 ± 0.001	0.1447 ± 0.0003	1.1368 ± 0.0009	13629 ± 17	14.77 ± 0.04	1.1427 ± 0.0009
	310-M0011A- 6R-1W 24-35	mp	IS	mP	110.3	106.5	MC-ICPMS		2604.3 ± 0.3	0.091 ± 0.001	0.1464 ± 0.0005	1.1382 ± 0.0009	87580 ± 575	14.93 ± 0.06	1.1442 ± 0.0009

Location	IODP Sample ID	Coral Species	In situ / Reworked	Coralgal Assemblages	Depth (mbsl)	Corrected Depth	Analytical technique		^{238}U ppb	^{232}Th ppb	$(^{230}\text{Th}/^{238}\text{U})$	$(^{234}\text{U}/^{238}\text{U})$	$(^{238}\text{U}/^{232}\text{Th})$	Age ka (BP)	$(^{234}\text{U}/^{238}\text{U})_0$
310-M0021A- 13R-2W 66-75		mp	IS	mP	101.9	98.4	TIMS	#1	2441.3 ± 3.1	0.385 ± 0.001	0.1381 ± 0.0004	1.1396 ± 0.0007	19403 ± 43	14.01 ± 0.05	1.1453 ± 0.0007
							TIMS	#2	2429.0 ± 3.1	0.481 ± 0.001	0.1381 ± 0.0003	1.1394 ± 0.0005	15441 ± 31	14.02 ± 0.03	1.1451 ± 0.0005
310-M0021A- 17R-1W 13-19		bp	IS	PP	107.6	104.0	TIMS		3798.7 ± 5.2	5.560 ± 0.010	0.1409 ± 0.0004	1.1386 ± 0.0010	2088 ± 5	14.33 ± 0.04	1.1443 ± 0.0010
310-M0021B- 16R-1W 39-44		rbp	IS	PP	107.2	103.6	TIMS		3059.7 ± 3.9	0.486 ± 0.001	0.1412 ± 0.0002	1.1396 ± 0.0004	19246 ± 37	14.35 ± 0.04	1.1454 ± 0.0005
310-M0023A- 5W-1R 45-52		mp	IS	mP	75.0	71.9	TIMS		2361.5 ± 3.0	0.299 ± 0.001	0.1232 ± 0.0003	1.1426 ± 0.0007	24120 ± 68	12.37 ± 0.04	1.1477 ± 0.0007
310-M0023A- 6R-1W 117-146		mp	IS	mP	77.6	74.5	TIMS		2635.1 ± 3.5	0.720 ± 0.001	0.1240 ± 0.0002	1.1421 ± 0.0006	11188 ± 23	12.46 ± 0.02	1.1472 ± 0.0006
310-M0023A- 11R-1W 22-31		rbp	IS	PP	85.9	82.5	TIMS		2984.8 ± 3.9	1.296 ± 0.002	0.1332 ± 0.0002	1.1408 ± 0.0007	7037 ± 14	13.46 ± 0.02	1.1463 ± 0.0008
310-M0023A- 11R-2W 112-121		bp	IS	PP	88.0	84.6	TIMS		2512.9 ± 3.2	3.625 ± 0.006	0.1342 ± 0.0002	1.1414 ± 0.0005	2118 ± 5	13.57 ± 0.02	1.1469 ± 0.0005
310-M0023A- 12R-1W 32-38		rbp	IS	PP	88.7	85.3	TIMS		2924.3 ± 3.7	2.230 ± 0.003	0.1342 ± 0.0002	1.1403 ± 0.0005	4007 ± 8	13.58 ± 0.02	1.1458 ± 0.0005
310-M0023A- 12R-1W140-145		ml	IS	PP	89.8	86.3	TIMS		2581.3 ± 3.3	2.672 ± 0.004	0.1356 ± 0.0002	1.1403 ± 0.0005	2953 ± 6	13.74 ± 0.02	1.1459 ± 0.0005
310-M0023A- 13R-2W 32-37		bpo	IS	PP*	92.0	88.4	TIMS		2667.1 ± 3.4	0.456 ± 0.001	0.1410 ± 0.0003	1.1404 ± 0.0005	17869 ± 42	14.31 ± 0.04	1.1462 ± 0.0005
310-M0023A- 14R-1W 0-20		rbp	Rew		93.4	89.7	TIMS		2651.4 ± 3.4	1.295 ± 0.002	0.1435 ± 0.0002	1.1401 ± 0.0005	6256 ± 12	14.59 ± 0.02	1.1461 ± 0.0006
310-M0023B- 12R-1W 30-33		fm	IS	PP*	90.4	86.9	TIMS		3721.5 ± 4.8	1.710 ± 0.002	0.1379 ± 0.0001	1.1397 ± 0.0006	6652 ± 13	13.99 ± 0.02	1.1454 ± 0.0006
310-M0023B- 12R-2W 113-127		rbp	IS	PP*	91.8	88.2	TIMS	#1	2707.0 ± 3.5	0.459 ± 0.001	0.1404 ± 0.0002	1.1395 ± 0.0004	18036 ± 35	14.27 ± 0.02	1.1453 ± 0.0005
							TIMS	#2	2651.9 ± 3.5	0.540 ± 0.001	0.1407 ± 0.0002	1.1395 ± 0.0009	15013 ± 29	14.30 ± 0.03	1.1453 ± 0.0009
310-M0023B- 15R-1W 0-5		rbp	Rew		96.6	93.0	TIMS		2663.1 ± 3.4	1.527 ± 0.002	0.1406 ± 0.0002	1.1397 ± 0.0006	5328 ± 11	14.28 ± 0.03	1.1455 ± 0.0006
310-M0024A- 1R-1W 36-41		mm	IS	AFM	91.3	88.2	TIMS		4119.3 ± 5.2	7.361 ± 0.014	0.1226 ± 0.0003	1.1417 ± 0.0006	1710 ± 4	12.31 ± 0.03	1.1468 ± 0.0006
310-M0024A- 4R-1W 137-141		bpo	IS	AFM	95.4	92.0	TIMS		2848.8 ± 3.6	10.606 ± 0.017	0.1342 ± 0.0004	1.1419 ± 0.0006	821 ± 2	13.56 ± 0.04	1.1475 ± 0.0006
310-M0024A- 10R-1W 65-75		rbp	IS	PM*	108.7	105.1	TIMS		2727.2 ± 3.6	0.198 ± 0.000	0.1433 ± 0.0005	1.1392 ± 0.0009	42037 ± 113	14.58 ± 0.05	1.1451 ± 0.0010
310-M0024A- 10R-1W 98-116		rbp	IS	PM*	109.1	105.4	TIMS		2619.9 ± 3.4	1.176 ± 0.002	0.1436 ± 0.0002	1.1393 ± 0.0005	6807 ± 14	14.61 ± 0.03	1.1452 ± 0.0005
310-M0024A- 10R-2W 69-72		bp	IS	mP*	110.2	106.6	TIMS		2832.4 ± 3.6	0.988 ± 0.001	0.1448 ± 0.0002	1.1388 ± 0.0005	8763 ± 17	14.75 ± 0.03	1.1448 ± 0.0005
310-M0024A- 11R-2W 23-38		mp	IS	mP	112.9	109.2	TIMS	#1	2555.4 ± 3.2	0.420 ± 0.001	0.1470 ± 0.0002	1.1392 ± 0.0006	18615 ± 36	14.99 ± 0.03	1.1452 ± 0.0006
							TIMS	#2	2557.7 ± 3.2	0.143 ± 0.000	0.1472 ± 0.0006	1.1394 ± 0.0005	54595 ± 147	15.01 ± 0.07	1.1454 ± 0.0005
310-M0024A- 13R-1W 32-41		mp	IS	mP	116.0	112.3	TIMS		2701.0 ± 3.5	0.580 ± 0.001	0.1485 ± 0.0003	1.1393 ± 0.0007	14238 ± 30	15.15 ± 0.03	1.1454 ± 0.0007
310-M0024A- 14R-1W 24-28		mp	IS	mP	116.9	113.1	TIMS	#1	2583.1 ± 3.3	0.406 ± 0.001	0.1487 ± 0.0006	1.1391 ± 0.0008	19461 ± 48	15.18 ± 0.06	1.1452 ± 0.0008
							TIMS	#2	2393.0 ± 3.0	0.119 ± 0.000	0.1494 ± 0.0003	1.1393 ± 0.0006	61623 ± 172	15.25 ± 0.04	1.1454 ± 0.0007
310-M0024A- 15R-1W 16-20		rbp	Rew	PM	118.6	114.7	TIMS		3001.9 ± 3.8	2.154 ± 0.004	0.1538 ± 0.0003	1.1385 ± 0.0005	4259 ± 9	15.74 ± 0.03	1.1448 ± 0.0005
310-M0025B- 9R-1W 0-30		mp	IS	mP	112.8	109.1	MC-ICPMS		2652.9 ± 0.4	0.147 ± 0.001	0.1447 ± 0.0005	1.1387 ± 0.0009	55134 ± 362	14.74 ± 0.06	1.1446 ± 0.0009
310-M0025B- 9R-2W 60-70		mp	IS	mP	114.6	110.9	TIMS		2522.2 ± 3.2	0.296 ± 0.000	0.1453 ± 0.0003	1.1389 ± 0.0005	26008 ± 54	14.80 ± 0.03	1.1448 ± 0.0006
310-M0025B- 10R-1W 0-5		mp	IS	mP	114.8	111.1	TIMS		2492.5 ± 3.2	0.295 ± 0.000	0.1463 ± 0.0002	1.1394 ± 0.0005	25855 ± 50	14.90 ± 0.02	1.1454 ± 0.0005
310-M0025B- 11R-1W 70-74		em	IS	mP*	117.5	113.7	TIMS		2689.1 ± 3.5	0.820 ± 0.001	0.1499 ± 0.0002	1.1391 ± 0.0008	10022 ± 21	15.31 ± 0.02	1.1453 ± 0.0008
310-M0026A- 5R-1W 4-18		mp	IS	mP	114.5	110.8	TIMS		2517.2 ± 3.2	0.330 ± 0.001	0.1445 ± 0.0002	1.1392 ± 0.0005	23347 ± 77	14.72 ± 0.02	1.1451 ± 0.0006
310-M0026A- 5R-1W 117-127		mp	IS	mP	115.6	111.9	TIMS		2731.3 ± 3.6	0.519 ± 0.001	0.1458 ± 0.0003	1.1388 ± 0.0006	16077 ± 34	14.85 ± 0.03	1.1448 ± 0.0006
Faaa															
310-M0019A- 10R-1W 20-28		mp	IS	mP	81.8	78.8	MC-ICPMS		2626.3 ± 0.5	0.251 ± 0.004	0.1182 ± 0.0002	1.1410 ± 0.0010	31932 ± 507	11.86 ± 0.02	1.1458 ± 0.0010
310-M0020A- 2R-1W 31-32		pa	IS	mP	85.6	83.1	MC-ICPMS		4433.0 ± 5.6	0.775 ± 0.014	0.1001 ± 0.0004	1.1401 ± 0.0018	17470 ± 309	9.96 ± 0.04	1.1441 ± 0.0019
310-M0020A- 3R-1W 19-23		mp	?	mP	87.0	84.3	MC-ICPMS		3160.5 ± 4.1	1.376 ± 0.024	0.1067 ± 0.0004	1.1424 ± 0.0018	7015 ± 124	10.63 ± 0.04	1.1468 ± 0.0019
310-M0020A- 16R-1W 55-66		mp	IS	mP	104.5	101.0	MC-ICPMS		3189.7 ± 4.0	1.775 ± 0.031	0.1357 ± 0.0005	1.1414 ± 0.0018	5489 ± 97	13.72 ± 0.06	1.1471 ± 0.0019
310-M0020A- 20R-1W 140-150		bp	IS	PPM	111.2	107.6	MC-ICPMS		3579.7 ± 4.5	5.504 ± 0.097	0.1407 ± 0.0005	1.1440 ± 0.0018	1987 ± 35	14.24 ± 0.06	1.1499 ± 0.0019
310-M0020A- 21R-2W 13-20		rbp	IS	PPM	113.2	109.6	TIMS		2983.8 ± 3.8	0.459 ± 0.001	0.1395 ± 0.0004	1.1410 ± 0.0006	19888 ± 47	14.14 ± 0.05	1.1468 ± 0.0006
310-M0020A- 22R-2W 59-70		mp	IS	mP	115.8	112.1	MC-ICPMS		2795.4 ± 3.5	0.252 ± 0.004	0.1426 ± 0.0005	1.1408 ± 0.0018	33832 ± 598	14.49 ± 0.06	1.1467 ± 0.0019
310-M0020A- 23R-1W 56-64		mp	IS	mP	117.5	113.8	TIMS		2835.6 ± 3.7	0.167 ± 0.001	0.1423 ± 0.0005	1.1400 ± 0.0008	51786 ± 297	14.46 ± 0.06	1.1459 ± 0.0008
310-M0020A- 23R-2W 72-78		mp	IS	mP	119.0	115.3	MC-ICPMS		2868.6 ± 3.5	0.266 ± 0.005	0.1446 ± 0.0005	1.1387 ± 0.0008	32884 ± 582	14.73 ± 0.06	1.1446 ± 0.0009
310-M0020A- 24R-1W 28-38		mp	IS	mP	120.2	116.5	MC-ICPMS		2672.9 ± 3.9	0.131 ± 0.002	0.1435 ± 0.0005	1.1296 ± 0.0018	62207 ± 1101	14.74 ± 0.06	1.1352 ± 0.0019
310-M0020A- 24R-2W 38-42		ra	IS	PM	121.3	117.6	MC-ICPMS		3192.8 ± 4.0	0.559 ± 0.010	0.1436 ± 0.0005	1.1360 ± 0.0018	17444 ± 309	14.66 ± 0.06	1.1418 ± 0.0019

Additional References:

51   Inwood, J., Brewer, T., Braaksma, H. & Pezard, P. Integration of core, logging and drilling data in modern reefal carbonates to improve core location and recovery estimates (IODP Expedition 310). *Journal of the Geological Society* **165**, 585-596 (2008).

52   Camoin, G., Iryu, Y., McInroy, D. & Scientists, E. IODP Expedition 310 reconstructs sea-Level, climatic and environmental changes in the South Pacific during the Last Deglaciation. *Scientific Drilling* **5**, 4-12 (2007).

53   Abbey, E. *et al.* Variation in deglacial coralgal assemblages and their paleoenvironmental significance: IODP Expedition 310, "Tahiti Sea Level". *Global and Planetary Change* **76**, 1-15, doi:10.1016/j.gloplacha.2010.11.005 (2011).

54   Camoin, G. *et al.* Reef response to sea-level and environmental changes during the last deglaciation. IODP Expedition 310 "Tahiti Sea Level". *Submitted to Geology* (2012).

55   Montaggioni, L. F. *et al.* Continuous record of reef growth over the past 14 k.y. on the mid-Pacific island of Tahiti. *Geology* **25**, 862 (1997).

56   Montaggioni, L. F. & Bard, E. Continuous record of reef growth over the past 14 ky on the mid-Pacific island of Tahiti: Reply. *Geology* **26**, 479-480 (1998).

57   Cabioch, G., Camoin, G. F. & Montaggioni, L. F. Postglacial growth history of a French Polynesian barrier reef tract, Tahiti, central Pacific. *Sedimentology* **46**, 985-1000 (1999).

58   Cheng, H. *et al.* The half-lives of Uranium-234 and Thorium-230. *Chem. Geol.* **169**, 17-33 (2000).

59   Ludwig, K. R. Isoplot 3.00: A Geochronological Toolkit for Microsoft Excel. Geochronological Centre Special Publication. Berkeley (2003).

60   Sepulcre, S., Durand, N. & Bard, E. Mineralogical determination of reef and periplatform carbonates: calibration and implications for paleoceanography and radiochronology. *Global and Planetary Change* **66**, 1-9 (2009).

61   Currie, L. A. Detection and quantification limits: origins and historical overview. *Analytica Chimica Acta* **391**, 127-134, doi:10.1016/s0003-2670(99)00105-1 (1999).

62   Hughen, K. A. *et al.* Marine04 marine radiocarbon age calibration, 0-26 cal kyr BP. *Radiocarbon* **46**, 1059-1086 (2004).

63   Reimer, P. J. *et al.* Comment on "Radiocarbon calibration curve spanning 0 to 50,000 years BP based on paired ^{230}Th/^{234}U/^{238}U and ^{14}C dates on pristine corals" by R.G. Fairbanks et al. (Quaternary Science Reviews 24 (2005) 1781-1796) and "Extending the radiocarbon calibration beyond 26,000 years before present using fossil corals" by T.-C. Chiu et al. (Quaternary Science Reviews 24 (2005) 1797-1808). *Quaternary Science Reviews* **25**, 855 (2006).

64   Deschamps, P., Doucelance, R., Ghaleb, B. & Michelot, J. L. Further investigations on optimized tail correction and high-precision measurement of Uranium isotopic ratios using Multi-Collector ICP-MS. *Chem. Geol.* **201**, 141-160 (2003).

65   Stirling, C. H., Andersen, M. B., Potter, E. K. & Halliday, A. N. Low-temperature isotopic fractionation of uranium. *Earth Planet. Sci. Lett.* **264**, 208-225, doi:10.1016/j.epsl.2007.09.019|ISSN 0012-821X (2007).

66   Weyer, S. *et al.* Natural fractionation of ^{238}U/^{235}U. *Geochim. Cosmochim. Acta* **72**, 345-359 (2008).

67   Condon, D. J., McLean, N., Noble, S. R. & Bowring, S. A. Isotopic composition (U-238/U-235) of some commonly used uranium reference materials. *Geochim. Cosmochim. Acta* **74**, 7127-7143, doi:10.1016/j.gca.2010.09.019 (2010).

68   Bard, E. *et al.* U/Th and ^{14}C ages of corals from Barbados and their use for calibrating the ^{14}C time scale beyond 9000 years BP. *Nuclear Instrument and Methods in Physics Research* **B-52**, 461-468 (1990).

69   Delanghe, D., Bard, E. & Hamelin, B. New TIMS constraints on the uranium-238 and uranium-234 in seawaters from the main ocean basins and the Mediterranean Sea. *Marine Chemistry* **80**, 79-93 (2002).

70   Andersen, M. B., Stirling, C. H., Potter, E.-K. & Halliday, A. N. Toward epsilon levels of measurement precision on ^{234}U/^{238}U by using MC-ICPMS. *Int. J. Mass Spectrom.* **237**, 107-118 (2004).

71   Robinson, L. F., Belshaw, N. S. & Henderson, G. M. U and Th concentrations and isotope ratios in modern carbonates and waters from the Bahamas. *Geochim. Cosmochim. Acta* **68**, 1777-1789 (2004).

72   Cutler, K. B. *et al.* Radiocarbon calibration and comparison to 50 kyr BP with paired C-14 and Th-230 dating of corals from Vanuatu and Papua New Guinea. *Radiocarbon* **46**, 1127-1160 (2004).

73   Cabioch, G. *et al.* Continuous reef growth during the last 23 cal kyr BP in a tectonically active zone (Vanuatu, SouthWest Pacific). *Quaternary Science Reviews* **22**, 1771-1786 (2003).

74   Mason, A. J. & Henderson, G. M. Correction of multi-collector-ICP-MS instrumental biases in high-precision uranium-thorium chronology. *Int. J. Mass Spectrom.* **295**, 26-35, doi:10.1016/j.ijms.2010.06.016 (2010).

75   Le Roy, I. *Evolution des volcans en système de point chaud: île de Tahiti, archipel de la Société (Polynésie française)* Ph. D. Thesis, Université de Paris XI, (1994).

76   Pirazzoli, P. A. & MontaggionI, L. F. Holocene sea-level changes in french Polynesia. *Palaeogeography, Palaeoclimatology, Palaeoecology,* **68**, 153-175 (1988).

77   Thomas, A. L. *et al.* Assessing subsidence rates and paleo water-depths for Tahiti reefs using U-Th chronology of altered corals. *Marine Geology (in press)*, doi:10.1016/j.margeo.2011.12.006 (2012).

78   Fadil, A., Sichoix, L., Barriot, J.-P., Ortèga, P. & Willis, P. Evidence for a slow subsidence of the Tahiti Island from GPS, DORIS, and combined satellite altimetry and tide gauge sea level records. *Comptes Rendus Geoscience* **343**, 331-341 (2011).

79   Laborel, J. in *Sea-Level Research: a Manual for the Collection and Evaluation of Data* (Ed. O. Van de Plassche) 281-310 (Geo Books, 1986).

80   Chevalier, J. P. & Kuhlman, D. H. H. Les scléractiniaires de Moorea. Ile de la Société (Polynésie française). *J. Soc. Océan.* **34**, 55-75 (1983).

81   Kuhlman, D. H. H. & Chevalier, J. P. Les coraux (Scléractiniaires et Hydrocoralliaires) de l'atoll de Takapoto, îles Tuamotu: aspects écologiques. *Marine Ecology* **7**, 75-104 (1986).

82   Bouchon, C. Quantitative study of scleractinian coral communities of Tiahura Reef (Moorea Island, French Polynesia). Proceedings of the 5th International Coral Reef Congress 6, 279–284 (1985).

83   Bouchon, C. *Recherches sur des Peuplements de Scléractiniaires Indo-pacifiques (Mer Rouge, Océan Indien, Océan Pacifique).* Ph.D. Thesis. Université Aix-Marseille I (1996).

84   Faure, G. & Laboute, P. Formations récifales: I. Définition des unités récifales et distribution des principaux peuplements de Scléractiniaires. L'atoll de Tikehau : premiers résultats. *Océanographie* **22**, 108-136 (1984).

85   Sugihara, K., Yamada, T. & Iryu, Y. Contrasts of coral zonation between Ishigaki Island (Japan, northwest Pacific) and Tahiti Island (French Polynesia, central Pacific), and its significance in Quaternary reef growth histories. *SEALAIX'06 Meeting.* (eds G. Camoin, A. Droxler, C. Fulthorpe, & K Miller) 179-180 (Association des Sedimentologistes Français).

86   Durand, N. *et al.* New insight into the radiocarbon calibration based on ^{14}C and U-Th dating of corals drilled offshore Tahiti. *EGU General Assembly. Geophysical Research Abstracts* **12**.

87   Lighty, R. G., Macintyre, I. G. & Stuckenrath, R. Acropora palmata reef Framework: a reliable indicator of sea level in the western atlantic for the past 10,000 years. *Coral Reefs*, 125-130 (1982).

88   Goreau, T. F. & Wells, J. W. The shallow water scleractinia of Jamaïca: revised list of species and their vertical distribution range. *Bulletin of Marine Science*, 442-453 (1967).

89   Hubbard, D. K. in *Perspectives in Carbonate Geology: A Tribute to the Career of Robert Nathan Ginsburg*   (eds P Swart, G. P Eberli, & J McKenzie) 1-18 (Spec. Publ. Int. Assoc. Sedimentol. (41), 2009).

90   Bard, E. *et al.* Retreat Velocity of the North-Atlantic Polar Front During the Last Deglaciation Determined by C-14 Accelerator Mass-Spectrometry. *Nature* **328**, 791-794 (1987).

91   Bard, E. *et al.* Pleistocene sea levels and tectonic uplift based on dating of corals from Sumba Island, Indonesia. *Geophysical Research Letters* **23**, 1473-1476 (1996).

92   Bosscher, H. & Schlager, W. Computer simulation of reef growth. *Sedimentology* **39**, 503-512 (1992).

93   Bosence, D. & Waltham, D. Computer modeling the internal architecture of carbonate platforms. *Geology* **18**, 26-30 (1990).

94   Nakamura, T. & Nakamori, T. A geochemical model for coral reef formation. *Coral Reefs* **26**, 741-755 (2007).

95   Koelling, M. *et al.* SEALEX - Internal reef chronology and virtual drill logs from a spreadsheet-based reef growth model. *Global and Planetary Change* **66**, 149-159, doi:10.1016/j.gloplacha.2008.07.011 (2009).

96   Webster, J. M., Wallace, L. M., Clague, D. A. & Braga, J. C. Numerical modeling of the growth and drowning of Hawaiian coral reefs during the last two glacial cycles (0-250 kyr). *Geochemistry Geophysics Geosystems* **8**, doi:Q03011Artn q03011 (2007).

97   Camoin, G., Cabioch, G., Hamelin, B. & Lericolais, G. Rapport de mission SISMITA. 1-20 (Institut de recherche pour le développement, Papeete, Polynesia Francaise, 2003).

98   Nakada, M. & Lambeck, K. Glacial rebound and relative sea-level variations - a new appraisal. *Geophysical Journal of the Royal Astronomical Society* **90**, 171-224 (1987).

99   Johnston, P. The effect of spatially nonuniform water loads on prediction of sea-level change. *Geophysical Journal International* **114**, 615-634 (1993).

100   Okuno, J. & Nakada, M. Effects of water load on geophysical signals due to glacial rebound and implications for mantle viscosity. *Earth Planets and Space* **53**, 1121-1135 (2001).

101   Lambeck, K., Purcell, A., Johnston, P., Nakada, M. & Yokoyama, Y. Water-load definition in the glacio-hydro-isostatic sea-level equation. *Quaternary Science Reviews* **22**, 309-318 (2003).

102   Yokoyama, Y., De Deckker, P., Lambeck, K., Johnston, P. & Fifield, L. K. Sea-level at the Last Glacial Maximum: evidence from northwestern Australia to constrain ice volumes for oxygen isotope stage 2. *Paleogeogr. Paleoclimatol. Paleoecol.* **165**, 281-297 (2001).

103   Lambeck, K., Yokoyama, Y. & Purcell, T. Into and out of the Last Glacial Maximum: sea-level change during Oxygen Isotope Stages 3 and 2. *Quaternary Science Reviews* **21**, 343-360 (2002).

104   Lambeck, K., Yokoyama, Y., Johnston, P. & Purcell, A. Global ice volumes at the Last Glacial Maximum and early Lateglacial. *Earth Planet. Sci. Lett.* **181**, 513-527 (2000).

105   Farrell, W. E. & Clark, J. A. Postglacial Sea-Level. *Geophysical Journal of the Royal Astronomical Society* **46**, 647-667 (1976).